Hydraulic Fracturing Optimization: Experimental Investigation of Multiple Fracture Growth Homogeneity via Perforation Cluster Distribution

Hydraulic Fracturing Optimization: Experimental Investigation of Multiple Fracture Growth Homogeneity via Perforation Cluster Distribution

by

Andreas Michael, B.S.P.E.

Report

Presented to the Faculty of the Graduate School of

The University of Texas at Austin

in Partial Fulfillment

of the Requirements

for the Degree of

Master of Science in Engineering

The University of Texas at Austin

May 2016

To my parents and grandparents,

for helping me chase the American Dream

Acknowledgements

To my supervising professor Jon E. Olson I owe a great deal. That is for providing me with a project of commercial value within the petroleum industry and additionally for his support, directions and insights. Historically, exceptional graduate students have been supervised by the department's chairperson and it is thus an honor to have that happening to me.

Secondly, I want to thank my co-advisor Matthew T. Balhoff for his meticulous efforts in my research project, which I know did not fall into his primary specialty vicinity. He also helped me enormously in a time that was mentally very tough for me. The relationship between the graduate student and his advising professor(s) must be one of total harmony; in no case must the student feel challenged going to the laboratory for research work. He should instead feel invited, because there is something there to be gained.

Richard A. Schultz, my other co-advisor, was major to the project development, even though he came to the department while the project was already on its way. He trained my thinking process using his long experience from his participation in similar projects. I look forward working with both my advisor and my co-advisors in the future. Special thanks also go to his predecessor Jon T. Holder, who has been an awesome person to have in the laboratory with me. I wish him a happy retirement. My thanks go similarly to the technical and administrative staff which includes Darryl Nygaard, Glen Baum, Gary Miscoe and Dori Coy.

Finance was the biggest "chokepoint" I had to face in my higher education. Thus, I have to thank my parents, Michalis and Despo and grandparents for providing the route

for obtaining the funds needed to pursue my undergraduate degree here in Texas. I would not have reached this level without having my B.S.P.E. as a base. Also, I want to thank the donors of the eleven scholarships awards I received up to this point. This includes Chevron Corporation, Baker Hughes, Inc., the Pancyprian Association of Texas, the Houston Chapter of the International Association of Drilling Contractors, the Hellenic Professional Society of Texas and the Association of International Petroleum Negotiators.

Furthermore, I have to thank my friends in the department. I have never been in a place with higher concentration of intelligent people than the CPE and I do not think I ever will. It is my hope that by the time I retire, petroleum engineering will evolve to a coherent discipline of its own rather than amalgamation of other disciplines, which is what it seems to be now. For that to happen there has to be abundance of people both in industry and academia with deep as well as broad knowledge on petroleum engineering.

In particular, I wish to thank Vu Q. Nguyen and Arjang Gandomkar, who beyond being classmates from the early undergraduate years and outstanding petroleum engineers have also been the best gym buddies I ever had. I should also thank my officemates at CPE 3.142 for a great year and a half I had with them. These are Weiwei Wang, Valerie Gono, Hunjoo P. Lee, Mohsen Babazadeh, Kaimin Yue and Nana Asiamah.

Last but definitely not least, I would like to thank my twelve PetroBowl teammates from 2013 to 2015. It is great having our names "engraved" together on the wall of the world's premier petroleum engineering department.

To all I owe my gratitude.

Abstract

Hydraulic Fracturing Optimization: Experimental Investigation of Multiple Fracture Growth Homogeneity via Perforation Cluster Distribution

Andreas Michael, M.S.E.

The University of Texas at Austin, 2016

Supervisor: Jon E. Olson

Hydraulic fracturing is a reservoir stimulation technique used in the petroleum industry since 1947. High pressure fluid composed mainly of water generates cracks near the wellbore improving the surrounding permeability and enhancing the flow of oil and gas to the surface. Advances in hydraulic fracturing coupled with developments in horizontal drilling, have unlocked vast quantities of unconventional resources, previously believed impossible to be produced.

Fracture creation induces perturbations in the nearby in-situ stress regime suppressing the initiation and propagation of other fractures. Neighboring fractures are affected by this stress shadow effect, causing them to grow dissimilarly and they receive unequal portions of the injected fluid. Numerical simulation models have shown that non-uniform perforation cluster distributions with interior fractures closer to the exterior ones

can balance out these stress shadow effects, promoting more homogeneous multiple fracture growth compared to uniform perforation cluster distributions. In this work, laboratory-scale tests on three perforation configurations are performed on transparent specimens using distinctly colored fracturing fluids such that fracture growth can be observed. A normal faulting stress regime is replicated with the introduction of an overburden load in a confined space.

The results have shown that uniform perforation spacing configurations yields higher degree of fracture growth homogeneity, as maximum spacing minimizes stress shadow effects, compared to moving the middle perforation closer to the toe, or heel of the horizontal well. The experiments also showed a proclivity to form one dominant fracture. Time delay, neglected in most theoretical modelling studies, between fracture initiations is found to be a key parameter and is believed to be one of the major factors promoting this dominant fracture tendency along with wellbore pressure gradients. Moreover, in several cases, the injected bypassed perforation(s) to generate fracture(s) downstream. Finally, the compressibility of the fracturing fluid triggered somewhat unexpected transient pressure behavior.

The understanding of the stress shadow effects and what influences them could lead to optimization of hydraulic fracturing treatment design in terms of productivity and cost. Therefore, achieving more homogeneous multiple fracture growth patterns can be pivotal on the economic feasibility of several stimulation treatments.

Table of Contents

List of Tables

List of Figures

Chapter 1

Introduction

This chapter provides an introductory overview of this Master's Report. This includes general background information in Section 1.1, the scope and motivation of the research project in Section 1.2, as well as an overview of this report in Section 1.3.

1.1 Background

Hydraulic fracturing is a method used in oilfields since the 1940s for reservoir stimulation. It increases the rock permeability around the wellbore and improves its connection with the surrounding reservoir. This is accomplished by high pressure fluid injection which either creates cracks that propagate through the rock matrix, or by causing slippage along natural pre-existing fractures. Commonly, 20 to 40 fracture stages are placed in a horizontal well with four or more fractures pumped per stage simultaneously (Xu et al., 2013). The industrial impact of this technology has been massive and is responsible for the advances in the development of tight unconventional petroleum resources such as shale gas (Figure 1.1).

Fluids used include water, oils, and high viscosity gel and are typically varied per treatment and sometimes per stage. Previous research (Xu et al., 2013) has shown that low viscosity fluids tend to create larger fractures primarily in terms of height covering larger surface area but with limited width compared to high viscosity fluids. In addition, proppant particles (normally sand or ceramic) are pumped with the injection fluid for the purpose of filling up the created fractures, keeping them open after the fluid is flowed back and maintaining high fracture conductivity. The base fluid and proppant make up about 99.5 percent of the injection fluid and the balance consists of chemical additives such as acids and glycol, which helps to improve the quality of the stimulation process.

1

The creation of a fracture interacts with and alters the rock in-situ stresses, creating a "stress shadow" around it. This stress perturbation induced by the fracture stimulation affects nearby fractures causing them to grow and develop dissimilarly. This leads to a geometrically non-uniform treatment outcome and in many cases ineffective or prematurely terminated fractures (and therefore sub-optimal economics). Understanding stress shadowing and its effects is essential for optimizing the hydraulic fracture treatment design in terms of productivity and cost.

The interactions between simultaneously growing fractures are of great interest to the research and development branch of the petroleum industry. A technology of high commercial value, hydraulic fracturing is the subject of numerous studies and research projects both in the industry and academia. The goal is to understand what parameters influence hydraulic fracturing treatments, how, and to what extent.
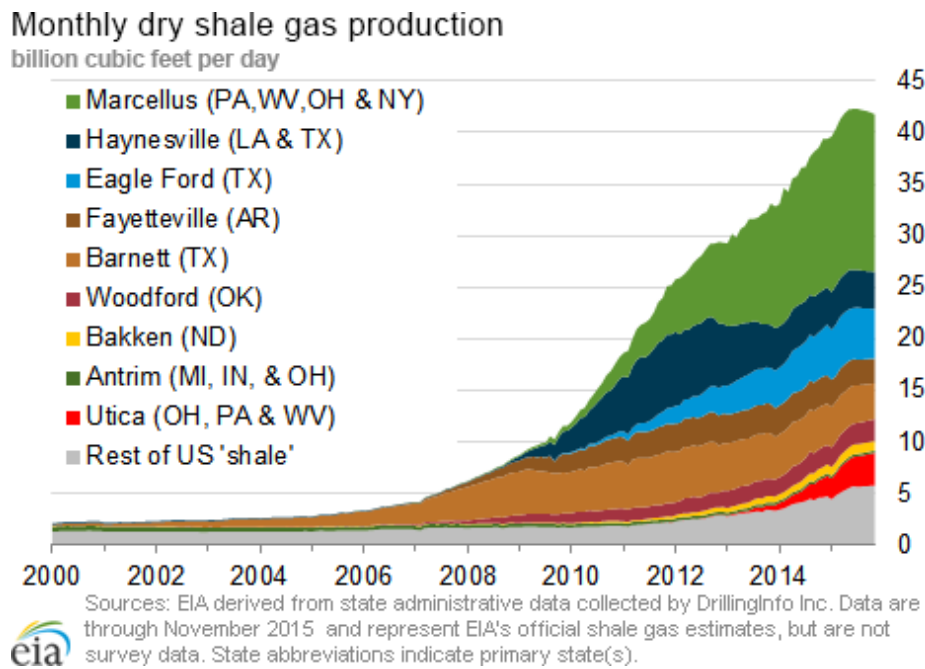
Figure 1.1 – United States natural gas production from shale basins (U.S. Energy Information Administration, 2015).

1.2 Research Motivation and Scope

The motivation for this experimental research is the conclusions of theoretical modelling studies that certain perforation cluster distribution arrays (see Figure 1.2) promote homogeneous fracture growth more than others.

Numerical simulations performed by Wu et al. (2015) for 4 perforation cluster (see Figure 1.3) arrays and by Peirce and Bunger (2015) for 5 perforation cluster arrays (see Figure 1.4a and b) indicate that at critical spacing patterns, the stress shadow effects are balanced out and uniform fracture development is promoted. Subsequently, these critical non-uniform cluster distributions were found to yield 46 to 74 percent more fracture surface area than uniform distributions.

Experiments were performed on three different cases of three perforation cluster arrays; one uniformly spaced (base case) and two non-uniformly spaced. **The hypothesis tested is that non-uniform perforation clusters can promote more homogeneous fracture growth compared to the uniform base case**. Unlike Peirce and Bunger (2015) and Wu et al. (2015) whose suggested non-uniform arrays are symmetric, our tested non-uniform arrays are non-symmetrical, in an attempt to compensate for the pressure gradients in the wellbore either by having the middle perforation (cluster) closer to either the heel, or the toe of the horizontal well.

Transparent materials are used along with distinctly colored fracturing fluids, enabling the visual monitoring and recording of fracture initiation and growth. Results are assessed for homogeneity based on the length dimension of each generated fracture.
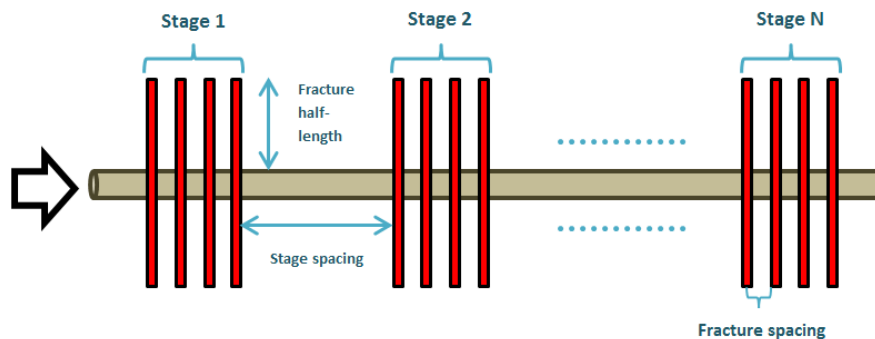
Figure 1.2 – Multiple fractures along a horizontal well.
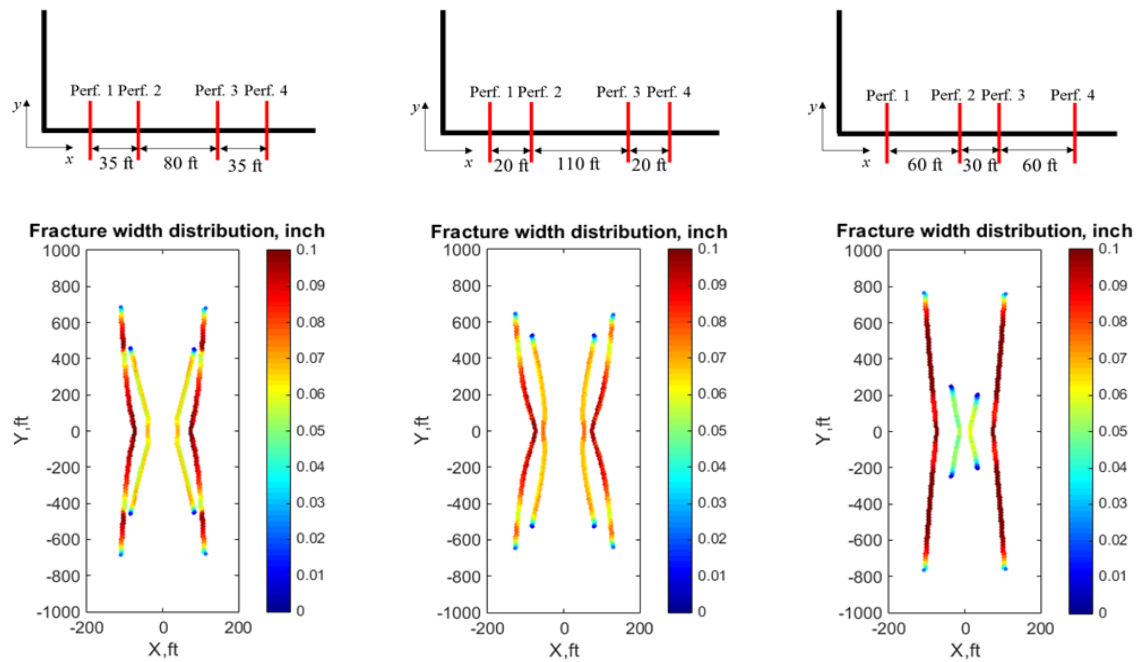
Figure 1.3 – Wu et al. (2015) simulations for 4 perforation (cluster) arrays.
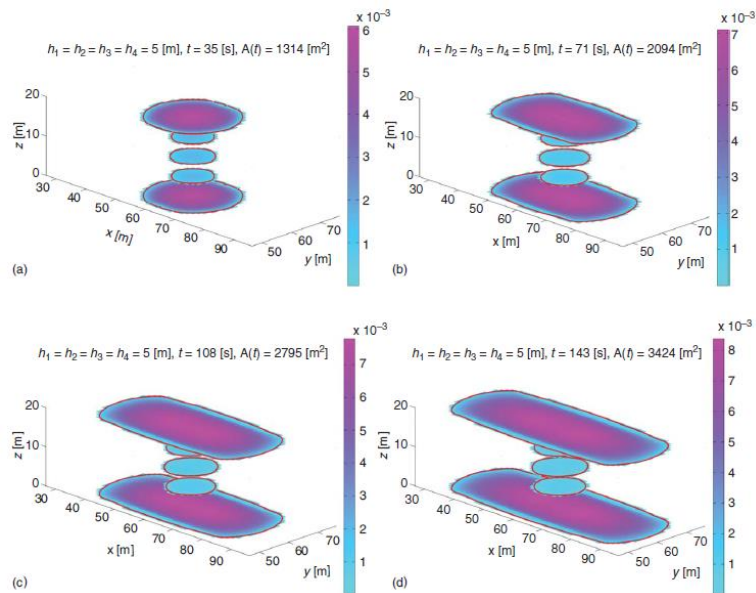
Figure 1.4a – Peirce and Bunger (2015) simulations for uniform 5 perforation arrays.

4
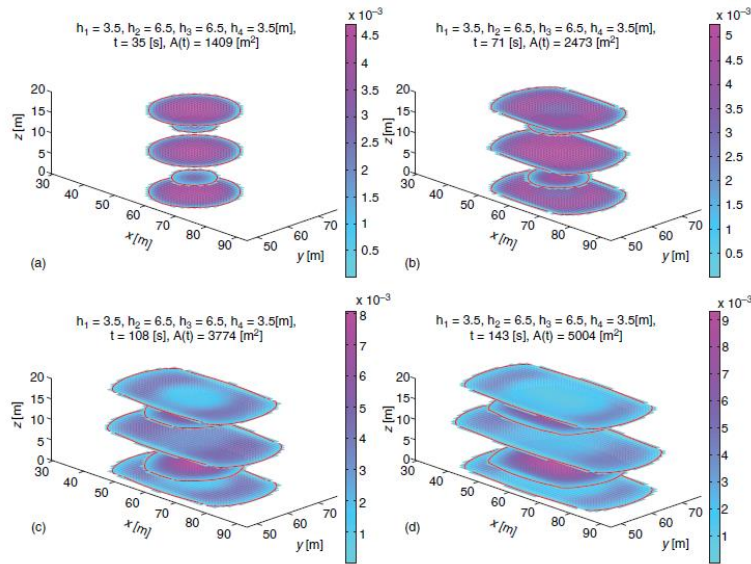
Figure 1.4b – Peirce and Bunger (2015) simulations for non-uniform 5 perforation arrays.

1.3 Report Overview

1.3.1 Organization

This report is organized into 5 chapters. Chapter 1 contains the introduction and a description of the method used for fracture growth homogeneity characterization. Chapter 2 provides a literature review on topics related to the research project. Chapter 3 gives a detailed description of the experimental methodology and outlines the experimental program. In Chapter 4 the results are illustrated, discussed and analyzed. Chapter 5 presents current conclusions and plans for future work. A complete list of citations is provided at the end in the Reference section.

1.3.2 Sign convention

Contrary to most texts on mechanics where tension is assumed to have positive direction, in rock mechanics compressive stresses are positive. In this report, to be

consistent with the existing literature on related topics, all equations are presented with the compressive stress component being positive.

Chapter 2

Literature Review

This chapter includes a summary of the existing scientific literature on the geomechanical principles behind the initiation, propagation and interaction of induced hydraulic fractures. It is divided into three main sections. Section 2.1 talks about subsurface in-situ stress regimes. Section 2.2 is related to hydraulic fracture characterization, and Section 2.3 is about simultaneous multiple hydraulic fracture interaction.

2.1   Subsurface In-situ Stress Regimes

The subsurface stress state can be fully characterized by three principal stresses acting along mutually orthogonal directions (S_1, S_2 and S_3, where $S_1 > S_2 > S_3$). In most cases, one of those stresses is aligned vertically and is denoted by S_v and the two others are horizontal. The largest horizontal stress is denoted by S_{Hmax} and the smaller by S_{hmin}. Figure 2.1 shows these stresses and their orientations. The principal stresses' relative magnitude with respect to each other dictates the subsurface stress regime and subsequently the direction induced fractures would propagate (Valko and Economides, 1995; Zoback, 2007; Crosby et al., 2002).

According to Anderson (1995) there are three main subsurface in-situ stress regimes:

i.   Normal faulting stress regime ($S_v > S_{Hmax} > S_{hmin}$)

ii.   Reverse (or thrust) faulting stress regime ($S_{Hmax} > S_{hmin} > S_v$)

iii. Strike-slip faulting stress regime ($S_{Hmax} > S_v > S_{hmin}$)

Each of those three regimes induces its corresponding fault tectonic movement. For example, normal faults are generated when normal faulting stress regime exists. In

accordance to their magnitudes they are also denoted by S_1, S_2 and S_3 from strongest to weakest.
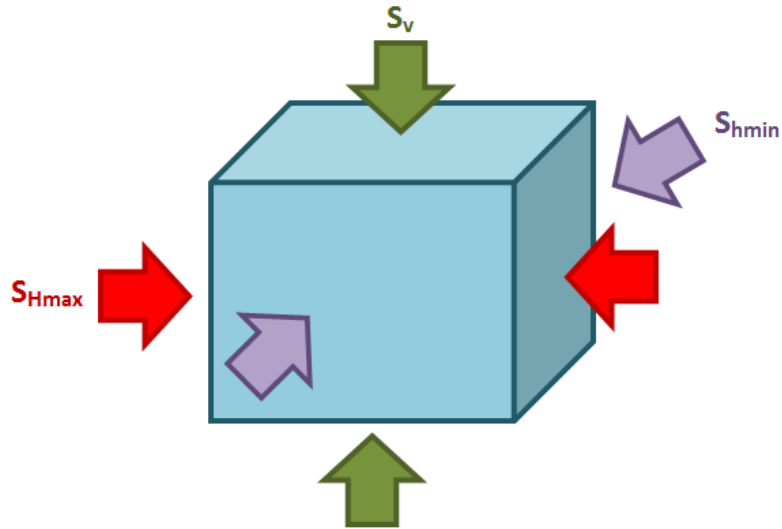
Figure 2.1 – The in-situ principal stresses acting on an element in the subsurface.

When the material is porous and pressurized fluid is present in the pores, this pore pressure counteracts the tectonic stresses. In this case the effective principal stresses have to be considered instead of the absolute tectonic stresses and these are denoted by σ_i,

$$\sigma_i = S_i - p_p \qquad (2.1)$$

where S_i is the corresponding subsurface principal stress and p_p is the pore pressure.

2.2 Hydraulic Fracture Characterization

2.2.1 Fracture Modes

There are three modes of fracture propagation, shown in Figure 2.2. Mode I refers to fractures where the normal stress direction is perpendicular the crack surface making the fracture propagate in the direction crack plane. Mode II fractures propagate between

crack faces and correspond to in-plane shear forces. Mode III fractures are shear displacements parallel to the crack plane induced by out-of-plane shear. In several cases a crack exhibits features of more than one mode, resulting in mixed mode fractures.
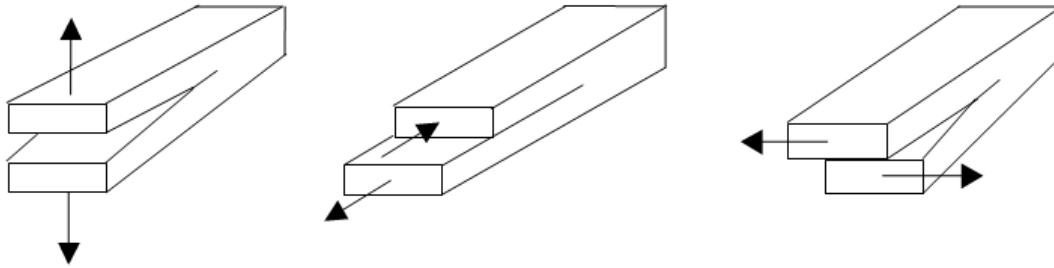
Figure 2.2 – The 3 modes of fracture. From left to right: Mode I, Mode II and Mode III.

2.2.2 Fracture Initiation, Propagation and Closure

Mode I "open mode" fractures open by doing work against the minimum (least compressive) principal stress, σ_3. For this study on simultaneous multiple fracture propagation from a horizontal wellbore, all fractures are assumed to be Mode I. Hence, there propagation direction is perpendicular to σ_3. The orientation of the wellbore (horizontal lateral) with respect to σ_3 determines whether the fractures generated will be longitudinal, or transverse (Valko and Economides, 1995; Crosby, 2002). Figures 2.3a and 2.3b show longitudinal and transverse fracture configurations, respectively.

As the treatment fluid is injected, the pressure at the perforations increases. When the wellbore pressure becomes equal to the breakdown, (or fracture initiation) pressure of the rock, a crack is created from where a fracture starts to grow. Figure 2.4 illustrates fracture initiation as wellbore pressure increases above a critical point. A number of studies throughout the years proposed different equations for measuring transverse fracture initiation pressure, for example Hubbert and Willis (1957) and Hoek and Brown (1980).
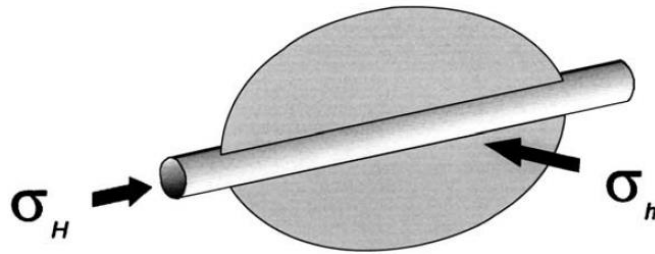
Figure 2.3a – Longitudinal fracture configuration (from Crosby et al., 2002), assuming normal faulting stress regime, so $\sigma_h = \sigma_3$.
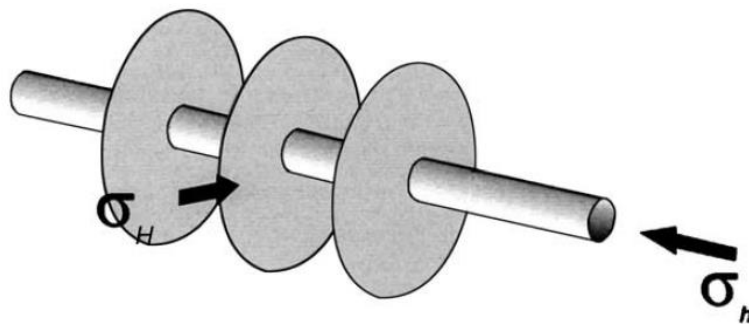
Figure 2.3b – Transverse fracture configuration (from Crosby et al., 2002). It assumes normal faulting stress regime, so $\sigma_h = \sigma_3$.

During a hydraulic fracture treatment the bottomhole pressure and fluid injection flow rate are carefully monitored. As shown in Figure 2.5 at a steady injection rate the bottomhole pressure increases linearly with time until a point where it becomes non-linear when pressure begins to leak into the formation. The pressure at which the leakage begins is known as the leak-off pressure (Fu, 2014). Despite the leak-off, the pressure continues to build up until the rock eventually breaks down and a crack forms. This is the breakdown pressure of the rock. Beyond that point further injection makes a fracture to extend from the induced crack. The pressure needed for the extension is the fracture propagation pressure, which is lower than both leak-off and breakdown pressures.

When injection ceases, the pressure inside the fracture begins to decline and it closes unless proppant has been pumped inside to keep it open. The fracture closure

stress is approximately equal to the minimum principal stress, σ_3. The fracture volume begins to increase after rock breakdown and keeps increasing during the fracture propagation process. It eventually either asymptotes to a maximum value after the pressure declines if proppant has been pumped, (as in Figure 2.5) or goes back toward zero as the fracture closes if proppant has not been pumped.

$$p<\sigma_2< \sigma_1$$

$$\sigma_2< P< \sigma_1$$

$$p<\sigma_3<\sigma_2< \sigma_1$$

$$\sigma_3<P<\sigma_2< \sigma_1$$
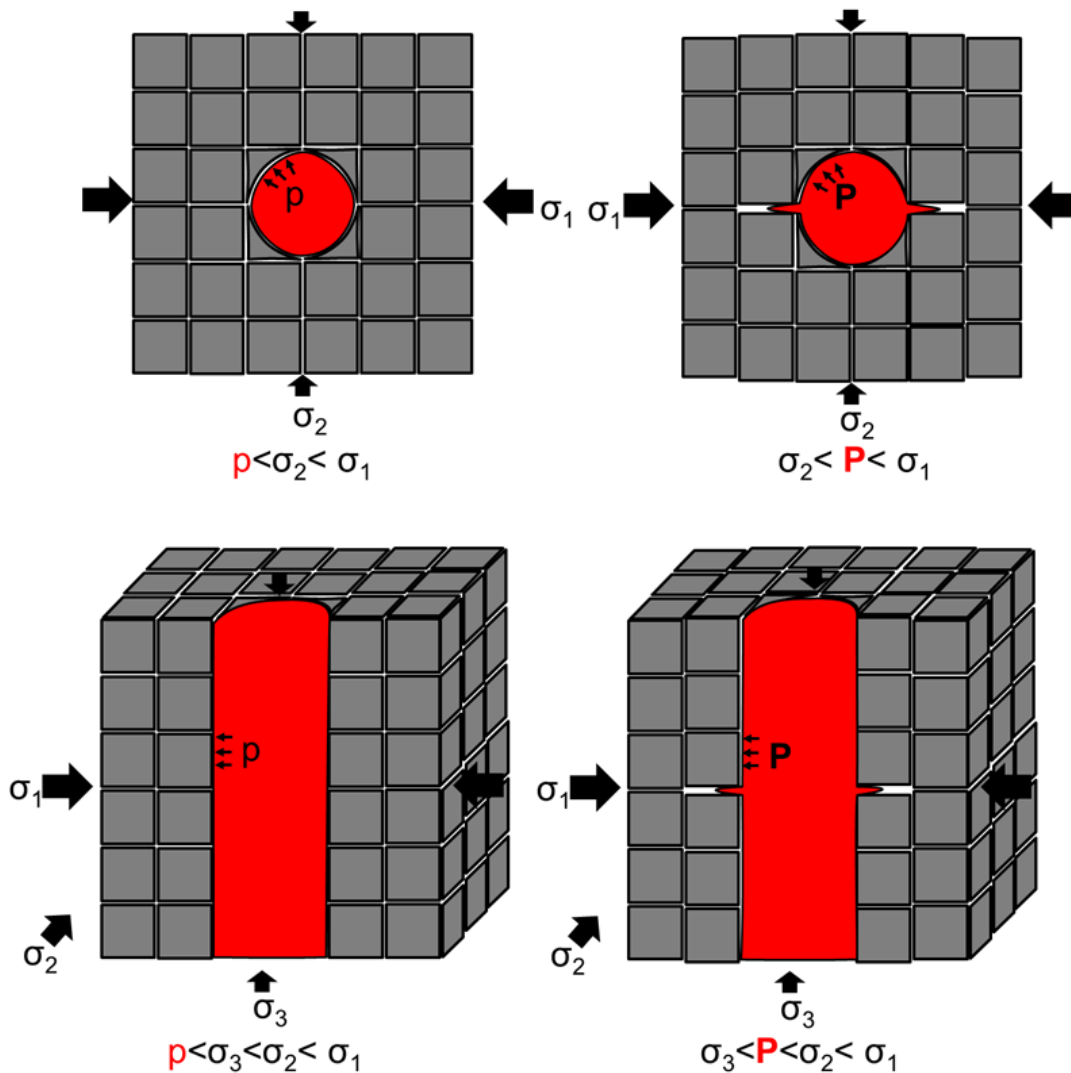
Figure 2.4 – Induced hydraulic fracture initiation when wellbore pressure (p) becomes bigger than the minimum principal stress, σ_3 (P).
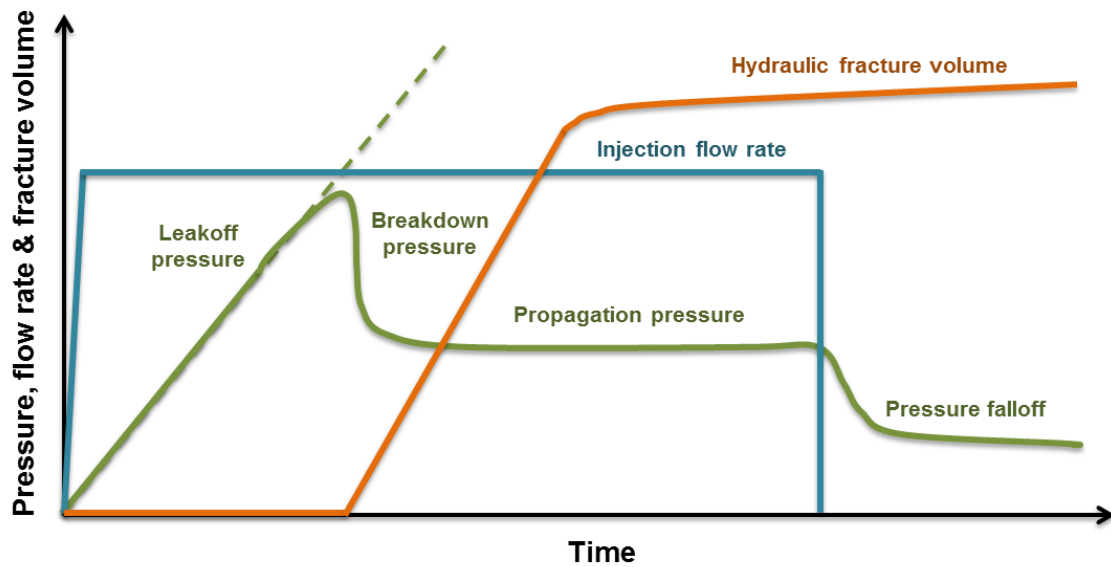
Figure 2.5 – Idealized parameters versus time plot during a hydraulic fracturing treatment.

Modelling of the pressure needed to initiate a fracture in relation to the near wellbore stresses was developed by Hubbert and Willis (1957) using Kirsch's (1898) stress concentrations at the wellbore wall and was modified by Haimson and Fairhurst (1967) to incorporate pore pressure and fluid flow. The equation for breakdown pressure, in normal faulting stress regime is the following;

$$P_b = S_{hmin} - 3_{Hmax} + T - p_p \tag{2.2}$$

$$P_{closure} = S_{hmin} - p_p = \sigma_{hmin} \tag{2.3}$$

T is the tensile strength of the material and p_p is the in situ pore pressure. This assumes vertical impact open borehole, vertical planar fracture orientation (normal faulting stress regime), homogeneous and isotropic rock matrix, which exhibits linearly elastic rock deformation and obeys the tensile stress failure criterion (Frash, 2014).

Assuming the rock to be impermeable as well as having zero pore pressure, then the tensile strength can, in theory, be computed with the expression,

12

$$T = P_b + 3S_{Hmax} - S_{hmin} \tag{2.4}$$

where the wellbore is aligned with S_v under normal faulting stress regime.

2.2.3 Fracture Geometry

The most widely used pseudo-3D fracture propagation geometries are the radial (or penny-shaped), Kristonovich-Geertsma-de Klerk (KGD) and Perkins-Kern-Nordgren (PKN) models, depicted on Figure 2.6a, b and c, respectively. Each model is more applicable than the others for different situations. For example PKN model is more accurate for longer fracture where changes in the height are negligible. Also, some models can be more applicable at different stages of propagation of a specific fracture. For instance, Peirce and Bunger (2015) in their numerical simulations used radial model for the earlier stages of the fracture propagation, leading to PKN geometry at the latter stages. The following brief descriptions of each model are based on Economides et al. (1994).

The radial model is a limiting one, where the fracture height is twice the radius ($\delta z = 2rf$) and is appropriate for small treatments in formations with thick pay zones, keeping the fracture away from any vertical barriers with an approximately circular shape. For this radial fracture propagation case with no leak-off, the radius, r_f can be calculated by,
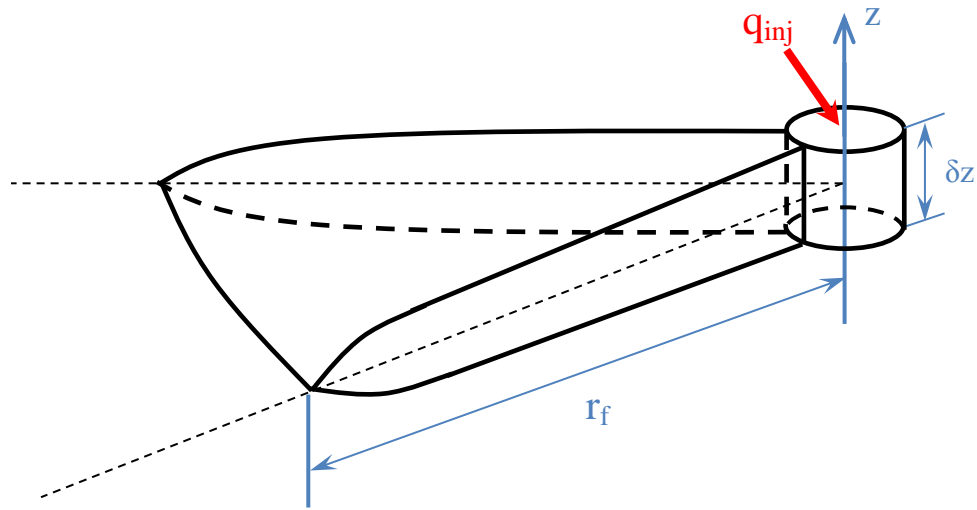
Figure 2.6a – Radial (or penny-shaped) fracture geometry.

$$r_f = 0.56 \left(\frac{G q_{inj}^3}{(1-v)\mu} \right)^{1/9} t^{4/9} \qquad (2.5)$$

where q_{inj} is the volumetric fluid injection rate, G is the shear modulus, v the Poisson's ratio, μ the fluid viscosity and t is the time from fracture initiation (Perkins and Kern, 1961; Geerstma and de Klerk, 1969).

The KGD model is applicable to short-length fractures where the fracture height is bigger than the length. The width stays constant along the entire height of the fracture. At the wellbore the width, $w_w(0, t)$ can be calculated from,
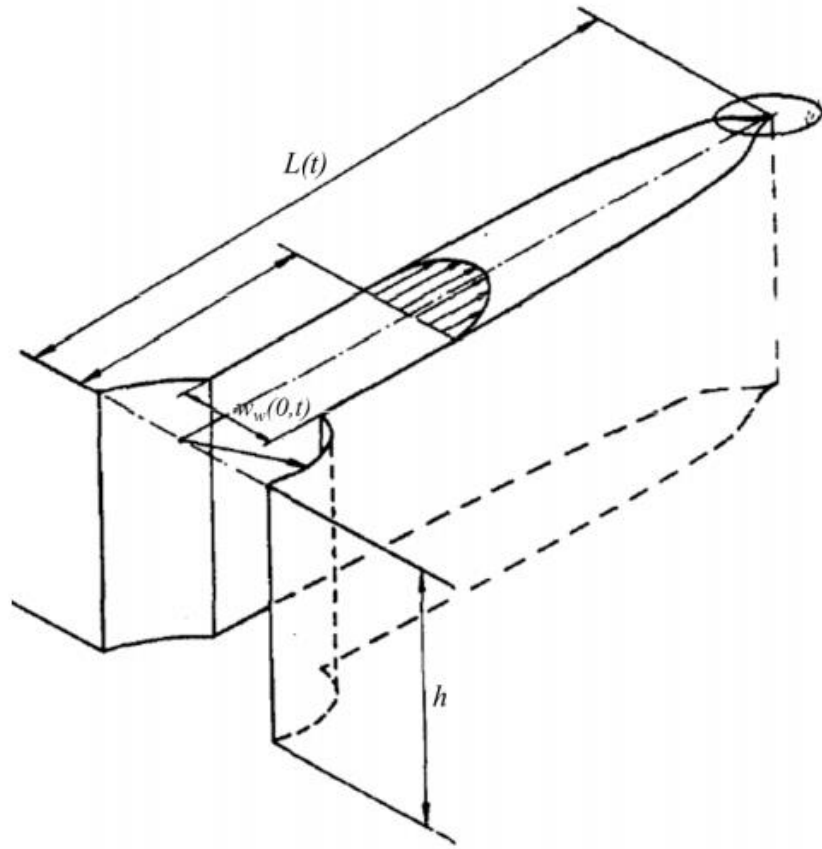
Figure 2.6b – Kristonovich-Geertsma-de Klerk (KGD) fracture geometry (from Geerstma and de Klerk, 1969).

$$w_w(0,t) = \frac{4(1-v^2)p_{net}^{average}L(t)}{E} \qquad (2.6)$$

$$p_{net}^{average} = p_{frac} - p_p \qquad (2.7)$$

where p_{frac} is the pressure of the fluid in the fracture, E is the Young's modulus of the formation and L is the fracture half length.

The PKN model is the opposite of KGD and is used when the fracture length is much larger than its height. The height is assumed to be constant along the entire fracture length, while the width varies from zero at the top and bottom apexes to a maximum value at the middle of the fracture height. Because of this width variation, PKN yields

lower fracture volumes than KGD modeling for the same fracture length. The width at any point along the length of the fracture can be calculated by,
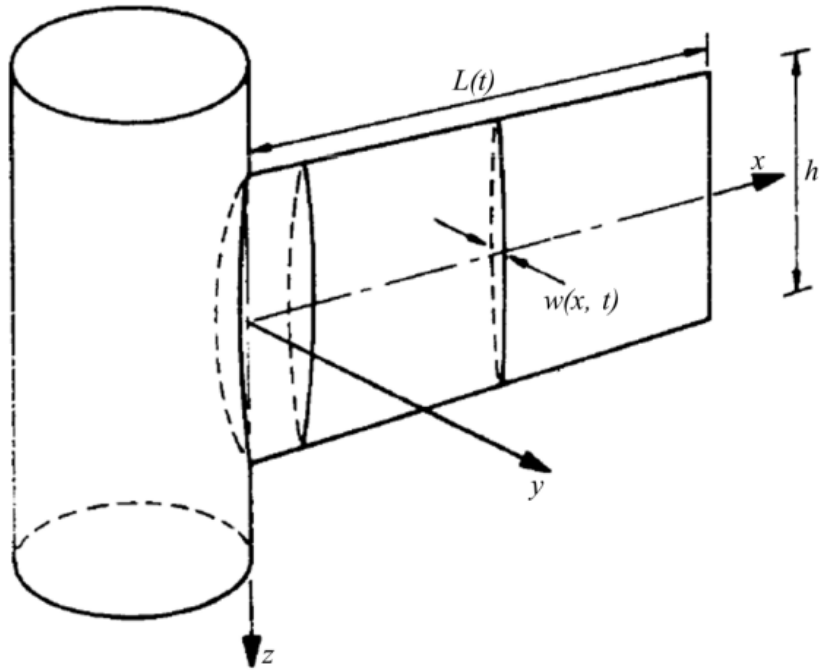
Figure 2.6c – Perkins-Kern-Nordgren (PKN) fracture geometry (from Nordgren et al., 1972).

$$w(x,t) = \frac{2(1-v^2)P_{net}(x,t)h}{E}$$
(2.8)

where p_{net} is the net pressure at any point along the length of the fracture and h is the fracture height.

16

2.3 Simultaneous Multiple Fracture Interaction

2.3.1 Stress Shadow Effect

Stress shadow effects have been studied extensively in the scientific and engineering communities. The potential gains from understanding of the stress shadow behavior and managing it, balancing its effects, are enormous.

2.3.1.1 Field Studies

Microseismic mapping results (Fisher et al., 2004) have shown that induced stress (shadow) effects on multiple fracture propagation increases with the number of perforation clusters pumped per stage. Consequently, less than three perforation clusters per fracturing stage were recommended to avoid excessive induced stresses, (Fisher et al., 2004). Similarly, Miller et al. (2011) examined production logs from many horizontal wells from six United States shale basins and discovered that the number of perforation clusters did not significantly to increase natural gas production (see Figure 2.7). In some basins approximately two thirds of the production is produced from one third of perforation clusters (Miller et al., 2011). The underperformance was attributed to the increased induced stresses due to the small spacing between the clusters. Miller et al. (2004) concluded that the optimum spacing range between perforation clusters is between 75 and 175 feet.
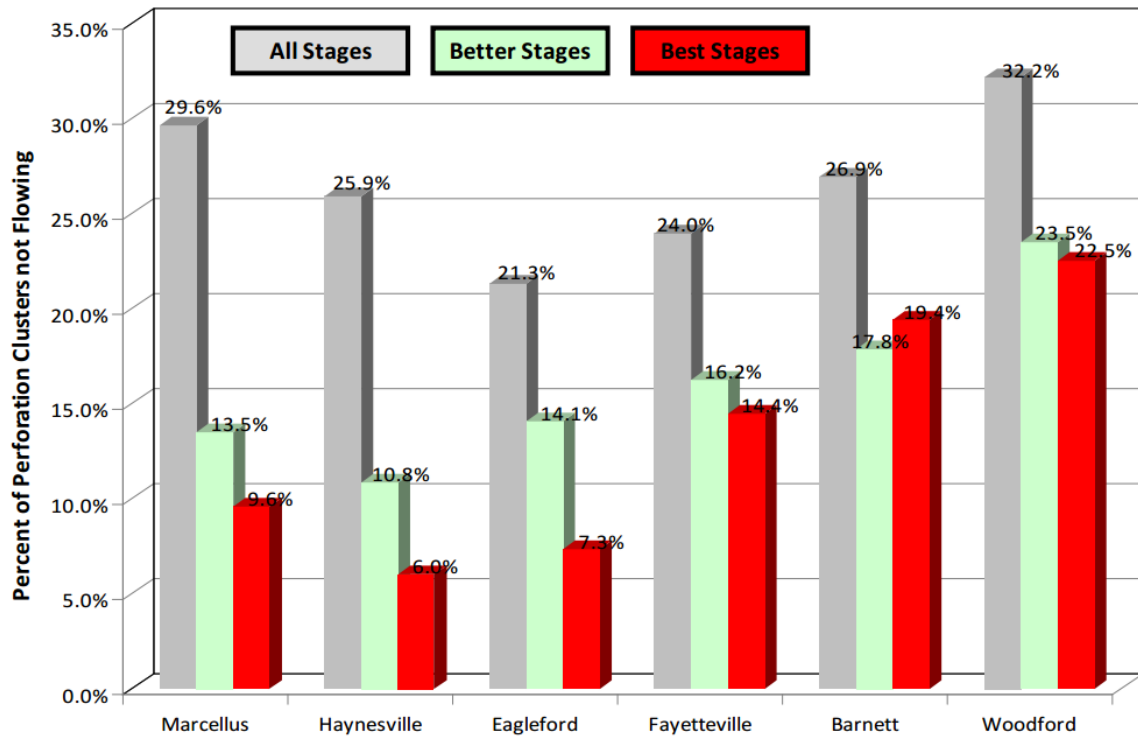
Figure 2.7 – Percentage of all perforation clusters that are not producing. The green bar is for fracture stages producing 110 to 150 percent above the average production rate. Red is for stages producing over 150 percent above the average rate (from Miller et al., 2011).

Real time downhole monitoring data studies have indicated restrictions of fracture growth along the middle perforation clusters (Molenaar et al., 2012; Koskella et al., 2014). This was explained by uneven distribution of fracturing fluid favoring the outer perforations in horizontal wells with multiple fractures (Holley et al., 2010; Molenaar et al., 2012). This suggests low fracture growth homogeneity leading to heterogeneous production from these perforation clusters.

2.3.1.2 Numerical Simulations

Fracture geometry was found to depend in multiple fractured horizontal wells and to be a function of the injection rate, fluid viscosity and proppant friction and fracture spacing (Lolon et al., 2009; Bunger et al., 2012). Furthermore, although well productivity is expected to increase with the number of fracturing stages, as the stimulated reservoir

volume increases, a threshold exists above which marginal well productivity per additional fracturing stage diminishes (Lolon et al., 2009).

Stress shadow effects on the propagation of simultaneous multiple fractures from horizontal wells was also closely examined in various studies analyzing the propagation of the hydraulic fracture tip. Analyzing the effects on the surrounding in-situ stress regime, it was found that the maximum increase in the principal stresses is across the hydraulic fracture face in the S_3 direction (Nagel et al., 2014). Moreover, it was suggested that stress shadow decreases the shear stress behind the fracture tip (Nagel et al., 2014). Shin and Sharma (2014) used models showing fluid leak-off to increase reservoir pore pressure subsequently increasing the stresses around the growing fracture. As a result, the opening of one fracture increases the closure pressure (see "pressure falloff" in Figure 2.5) of its neighboring fractures affecting their growth and geometry. This makes the outer fractures near the heel and toe of the horizontal well to curve away from the wellbore. Inner fractures in the middle of the horizontal well however, experience propagation constraints leading to complex patterns (Shin and Sharma, 2014; Olson, 2008; Olson and Wu, 2012) as illustrated by Figure 2.8.
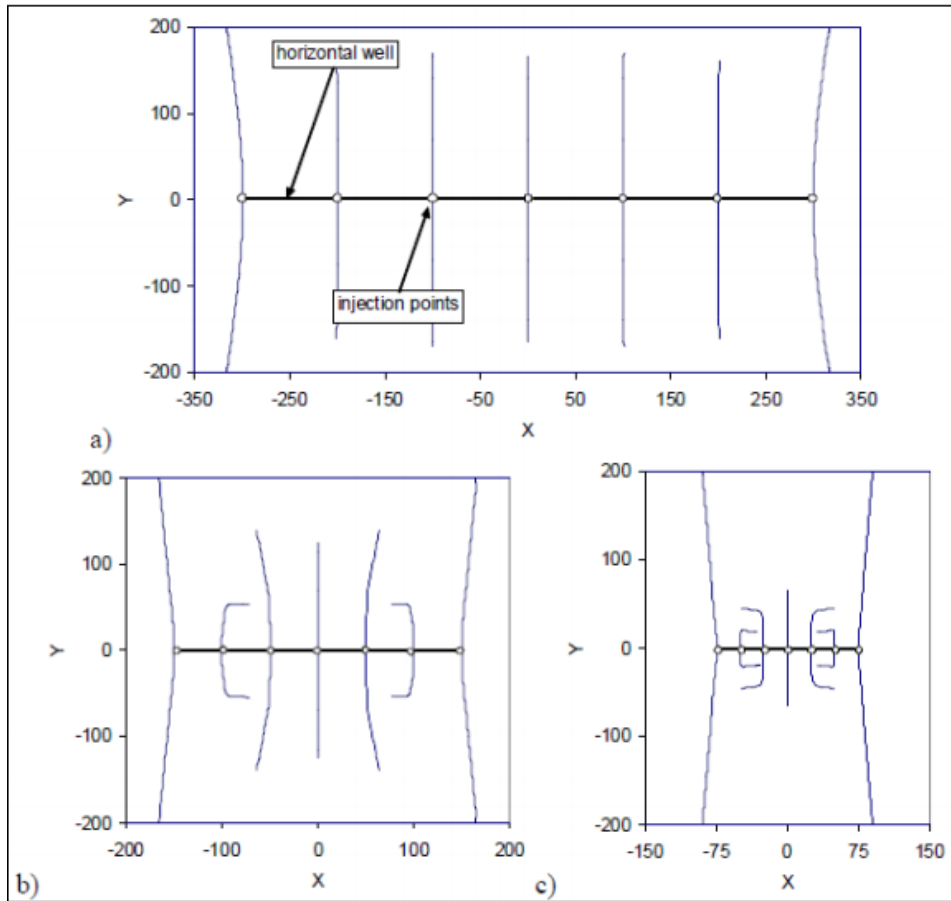
Figure 2.8 – Top view numerical simulation outputs at increasing stress shadow effect from (a) to (c) by decreasing the fracture spacing (from Olson, 2008).

Other analyses showed that shorter perforation cluster spacing, larger number of perforation clusters pumped per stage, higher fracturing fluid viscosity, larger fracture height and bigger formation Young's modulus all can increase the stress shadow effect (Shin and Sharma, 2014; Olson and Wu, 2012). However, higher fracturing fluid injection rate was found to decrease stress shadow (Shin and Sharma, 2014; Olson and Wu, 2012).

The role of the length of perforation intervals in the generation of multiple fractures was investigated as well. It was found that perforation clusters with interval length longer than four times the wellbore outer diameter are likely to generate multiple fractures at an elevated fracture treatment pressure (Soliman et al., 2004; Ketter et al.,

20

2006). All these results highlight the degree of heterogeneity that exists in multiple fracture growth from horizontal wells.

2.3.1.3 Laboratory Experiments

Laboratory testing on rock and hydrostone blocks (a mixture of Portland cement with gypsum plaster) was used in the past to examine the importance of perforation cluster design on the number of hydraulic fractures produced from each cluster.

The parameters highlighted are the perforation cluster interval length and the cluster spacing. El Rabaa (1989) found that perforation intervals shorter than four times the wellbore outer diameter are likely to produce only one single fracture (Figure 2.9). From the same set of experiments in the case of longitudinal fractures, opening perpendicular the trajectory of the wellbore, (Figure 2.3a) perforation cluster spacing of at least the length of the fracture was needed to avoid connection (El Rabaa, 1989).

Tests on hydrostone by Al Abbad (2014) showed that simultaneous multiple fracture propagation of similar length is operationally challenging. A tendency for the creation of one "dominant" fracture was observed. Moreover, closure of fractures in the middle segments prior to the far end ones, entraps fluid in these far end segments. This fluid remains unrecovered, contributing to partial recovery of injected fluids during flowbacks. Also, deflections in the induced fractures, either by the stress shadow effect, or interaction with pre-existing fractures creates regions of potential proppant bridging. This leads to pre-mature proppant screenouts.
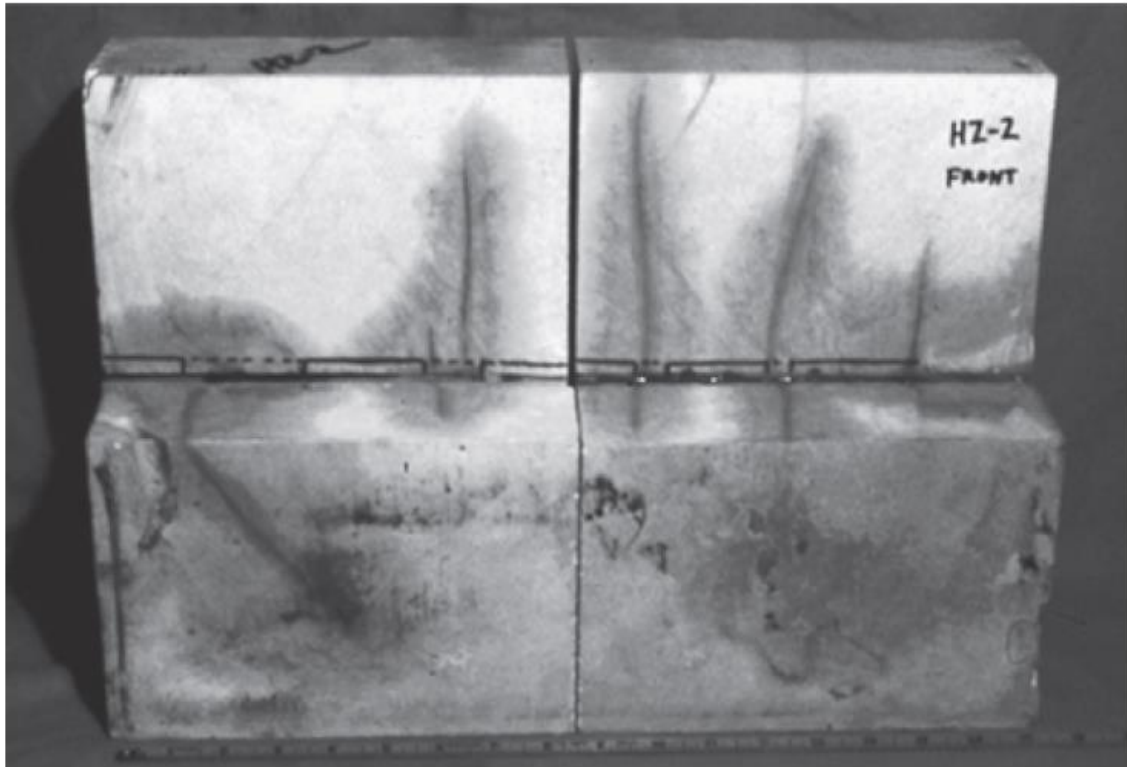
Figure 2.9 – Simultaneous multiple fracture propagation experiments using motor oil as fracturing fluid (from El Rabaa, 1989).

2.3.2 Stress Shadow Mitigation

Several techniques have been proposed through numerical simulations for the promotion of uniform fracture development (Wu et al., 2015). The first is the limited entry technique where the diameter or number of perforations is adjusted such that even fluid flow is achieved in all. The second is balancing the stress shadow effects using a non-uniform cluster array. This is the technique which is investigated experimentally in this report. The arrays proposed by the models have the interior fractures moved closer to the exterior ones, in an attempt to promote homogeneous fracture growth across all of the perforations.

Another proposed approach for mitigating the stress shadow effects in a horizontal well, is to have fractures initiated separately in a pre-defined sequence, instead of attempting to initiate them all simultaneously. It has been suggested that in the

22

presence of layers bounding the pay zone causing fracture containment that an alternative fracturing strategy 1-3-2-5-4 reduces the stress reorientation region, compared to consecutive fracturing 5-4-3-2-1, (shown in Figure 2.10) lessening the effect on the fractures' geometry and propagation.
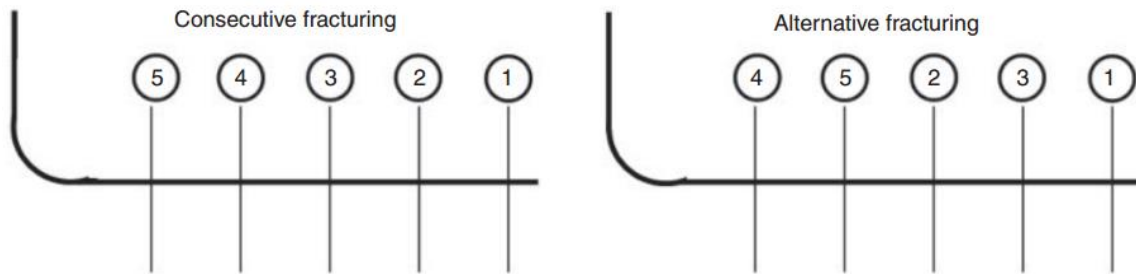
Figure 2.10 – Two fracturing sequencing techniques (a) consecutive 1-2-3-4-5 and (b) alternative 1-3-2-5-4 (from Roussel and Sharma, 2011).

Chapter 3

Experimental Methodology

This chapter provides a description of the methodology used in the experimental investigation. It is divided into four main sections. Section 3.1 discusses the materials used and the specimen preparation procedure and Section 3.2 talks about the experimental setup and the procedure followed for each test. Section 3.3 outlines the experimental program and Section 3.4 talks about the fracturing fluid selection. Section 3.5 provides a detailed example of the method used to characterize the fracture growth homogeneity in the experimental tests.

3.1   Materials and Preparation

3.1.1   Specimen Materials

The specimen material for the hydraulic fracturing experiments is edible Knox® Gelatin mixed with water. The mixture's brittle behavior makes it comparable to rock formations and its transparency enables visual inspection of fracture propagation. Moreover gelatin is elastic, impermeable and non-porous with homogeneous properties when prepared carefully. A perforated aluminum wellbore tube, bent having a vertical and horizontal section is used to inject the fracturing fluids into the specimen at a constant rate.

Experiments on hydraulic fracturing have been performed previously on polymethyl methacrylate/acrylic/PMMA (Frash et al., 2013; Frash et al., 2014) and hydrostone blocks (Bahorich, 2012; Al Abbad, 2014; Asiamah, 2015). Additionally, transparent urethane plastic (see Crystal Clear® Series in Reference Section) was considered for specimen material, but was not used in these experiments because it was not found to be as brittle as desired for the tests of this project.

Gelatin has a significantly lower Young's modulus, E estimated at 10-100 psi (Wu et al., 2008). This result in the breakdown pressure for gelatin being lower compared to the other two materials (hydrostone and PMMA) subsequently making fracture initiation is easier. Moreover, fracture geometry (length, width and height) is likely to be different in the gelatin mixture than in PMMA, or hydrostone according to models of fracture geometry in the literature, (Perkins and Kern, 1961; Nordgren, 1972) taking into consideration the specimen properties. Lower E would mean larger width, but smaller height and length.

3.1.2 Preliminary Testing of Specimen Materials

Urethane plastic, PMMA and gelatin mixture were the three materials considered for the experiments. Preliminary tests were performed, in an attempt to quantify some of their properties, including

    i.   Unconfined Compressive Stress (UCS) test for obtaining Young's modulus and yield stress

    ii.   Brazilian test for obtaining tensile strength

    iii.   Semi-Circular Bend (SCB) test for obtaining fracture toughness

Based on the results of those tests it was determined that gelatin of 7-8 percent by weight was the best candidate for the experiments. Note that not all three tests were possible to be performed on all three materials. Figure 3.1 shows Brazilian test and Figure 3.2 shows SCB test performed on a PMMA sample. Table 3.1 summarizes how the three specimen material candidates satisfy, or not, the properties required for our experimental program.

Table 3.1 – Properties of the media used in the tests.

Material	Transparency	Low fracture toughness, K_{IC}	Low tensile strength	Price affordable for multiple tests
Urethane plastic	✓	✗	✓	✗
PMMA	✓	✓	✗	✗
Gelatin (7-8% by weight)	✓	✓	✓	✓
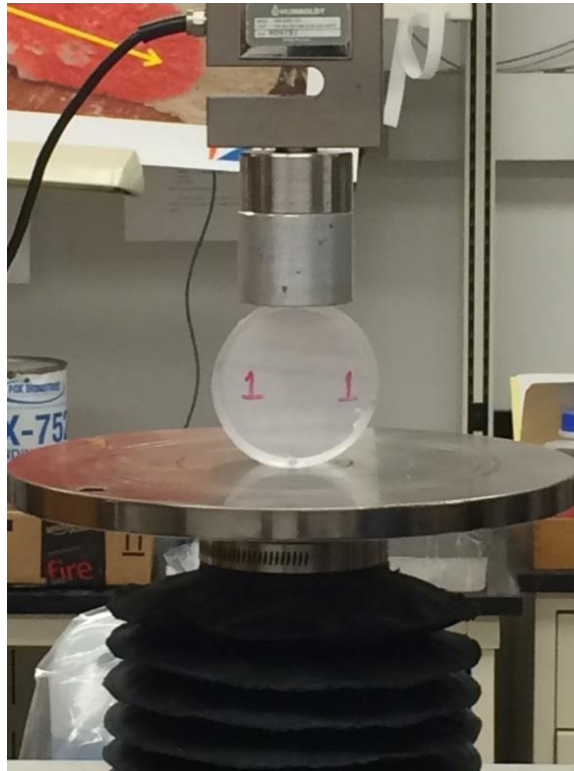
Figure 3.1 – Brazilian testing of PMMA, obtaining its tensile strength.
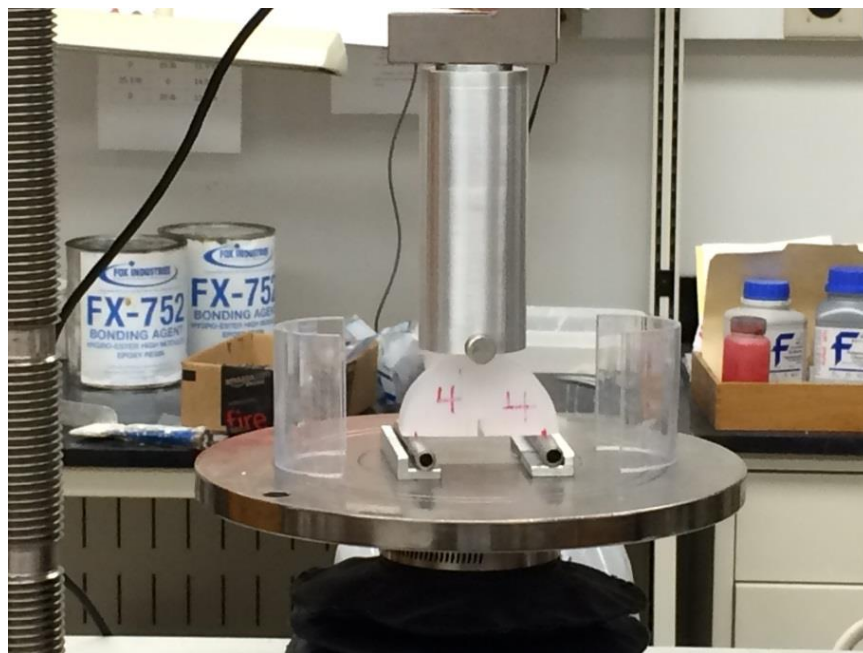
Figure 3.2 – SCB testing of PMMA, obtaining fracture toughness.

3.1.3   Specimen Preparation

Gelatin powder is added to hot water (near boiling point, 100 °C) and stirred. It is made sure that the gelatin powder concentration is about 7-8 percent by weight. The wellbore is placed in the container filled with the fracturing fluid to prevent penetration of liquid gelatin inside and is held in place with the help of a clamp (Figure 3.3a). Once the gelatin powder has completely dissolved, the liquid is poured into a plastic transparent container and placed on a refrigerator to cure at about 5°C overnight, or about 12 hours (Figure 3.3b). After the gelatin has cured the container is removed from the refrigerator (Figure 3.3c).
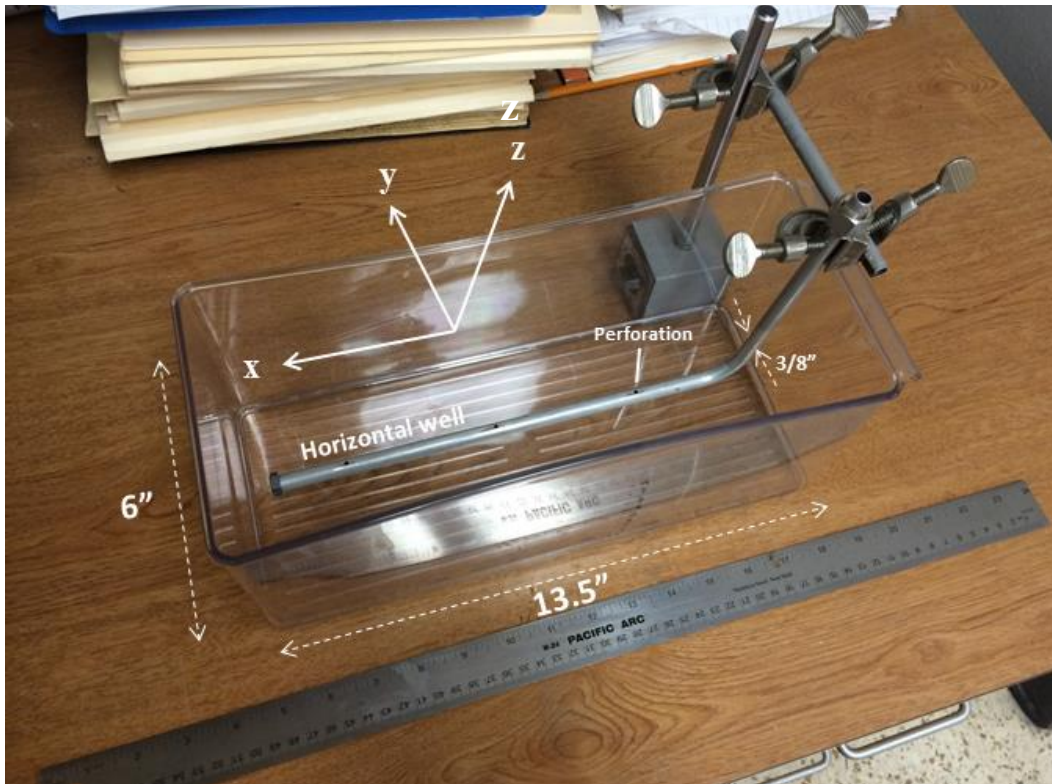
Figure 3.3a – Container with aluminum wellbore prior to addition of gelatin. The arrows show the direction of the axes x, y and z, assumed to be aligned with the principal stresses S_{Hmax}, S_{hmin} and S_v, respectively.

Figure 3.3b – Container with wellbore with gelatin placed in the refrigerator for curing.

Figure 3.3c – Cured gelatin with wellbore inside the container.

3.1.4 Wellbore Geometry and Perforations

The wellbore is an aluminum tube $3/8^{th}$ inch diameter OD with 0.065 inch wall thickness. The inclination angle is about 90 degrees. Perforations are made through $1/9^{th}$ inch holes drilled in the tubing facing up.

Different perforation spacing configurations are used both uniform and non-uniform. The spacing between perforations was made in accordance with the literature, (El Rabaa, 1989) such that multiple distinct fractures are promoted when perforation spacing is at least four times the wellbore tubing outer diameter.

3.1.5 Stress Conditions

The container provides confining pressure on the gelatin on the 2 horizontal directions x and y. The vertical part of the wellbore is aligned in the z-direction (see Figure 3.3b). Quantification of those confining stresses was not attempted. However, it was noted from fracture propagation that the shorter side, x is stronger than the longer side, y. In order to create normal faulting stress regime, an overburden load is applied via placing a mass on the gelatin surface. Through previous trial and error procedures, the gelatin was found to be able to withstand overburden pressures up to 0.20 psi (about 11.14 lb_m on a flat 11×5 in^2 surface). This stress is larger than the two horizontal stresses as indicated by fracture propagation as well. Even though this means that the fractures generated will be longitudinal to the wellbore, testing of the hypothesis is still possible due to the specimen dimensions and perforation spacing, which will allow multiple fractures generated to be distinct for a while, before they merge.

3.2 Experimental Setup and Testing Procedure

Fracturing fluid is placed in an accumulator and is injected into the specimen using Teledyne® ISCO pumps, which enable constant flow rate injection. Connections between the pump, accumulator and wellbore are made using $1/16^{th}$ inch high pressure

steel tubing. Figure 3.4 shows a schematic of the experimental setup. Data acquisition is performed using a custom made NI LabVIEW program with the data being further processed and analyzed using a code written in MATLAB.
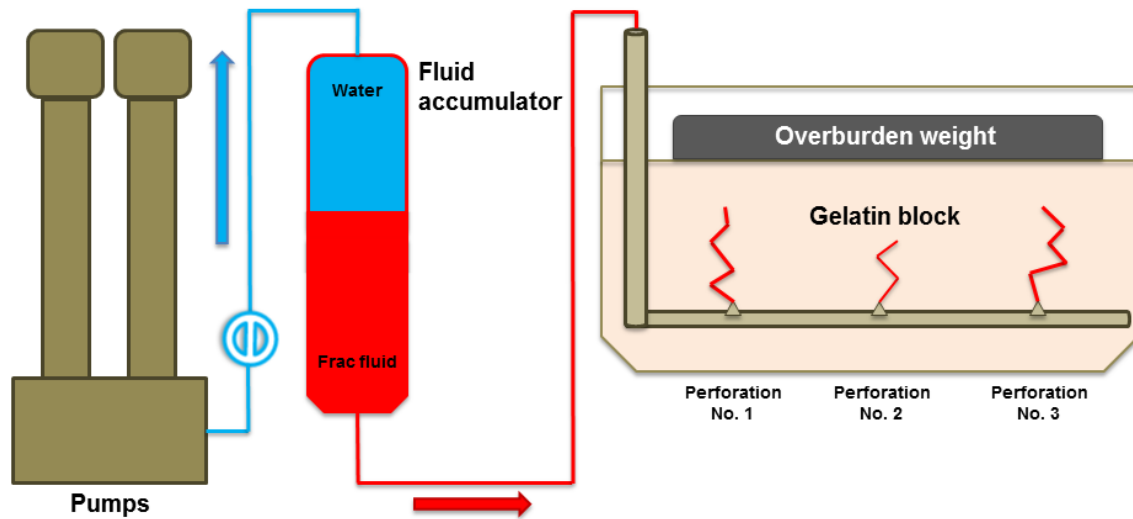
Figure 3.4 – Experimental setup.

Throughout the experimental program, this testing procedure was followed:

1. Synchronize all data acquisition and video equipment.
2. Make sure that the wellbore is filled with fracturing fluid and connect it to the tubing extended from the fluid accumulator.
3. Place overburden weight at the surface of gelatin. Do that gently, to avoid rupturing of the gelatin.
4. Close the outlet air valve at the bottom of the fluid accumulator.
5. Start the video recording equipment.
6. Start injection at a prescribed constant flow rate.
7. Stop injection as soon as the fracture reaches the specimen boundary.
8. Stop video recording and data acquisition.
9. Bleed out any residual pressure.
10. Photograph any final fracture key features in the specimen.
11. Disconnect the wellbore from the fluid accumulator and dispose the specimen.

3.3   Experimental Program

The experimental program consisted of multiple runs of three test cases of three perforation arrays. In all three cases the total length from the first perforation to the last is 7 inches. Case I is the base case with a uniformly spaced array with the perforations arranged 3.5 inches apart. Case II is a non-uniform array with the second perforation being 2 inches from the first and 5 inches from the last. Case III is also a non-uniform array, but the second perforation is 5 inches from the first and 2 inches from the last. Figures 3.5a-c show respectively Cases I to III. The experimental results, key observations and their conclusions are summarized and discussed in the following chapters.
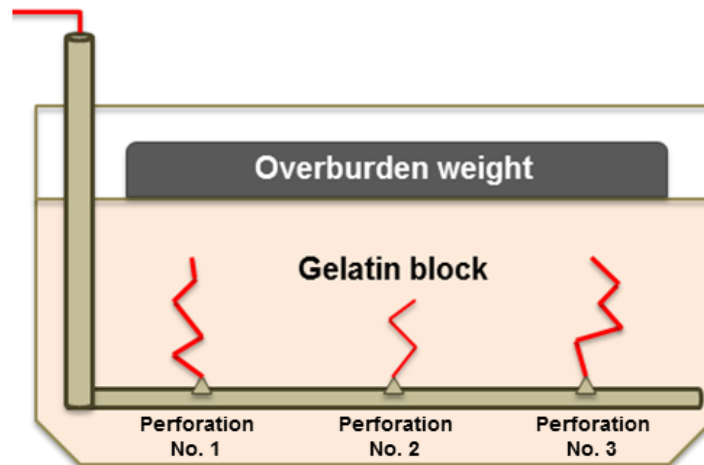
Figure 3.5a – Case I (base case): uniform array with perforations uniformly spaced.
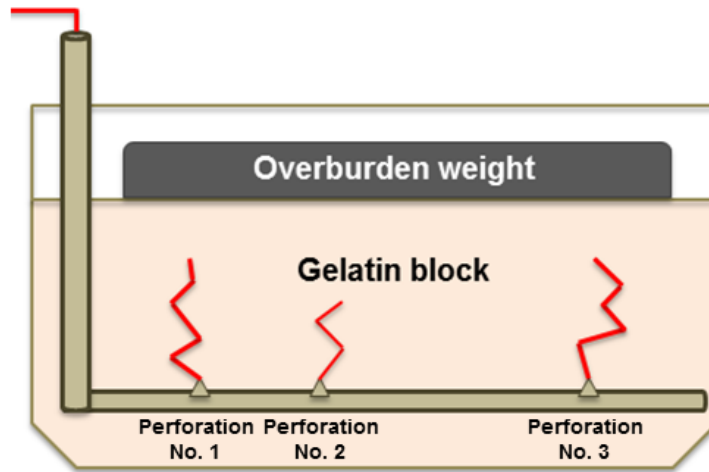
Figure 3.5b – Case II: non-uniform array with the second perforation closer to the first.
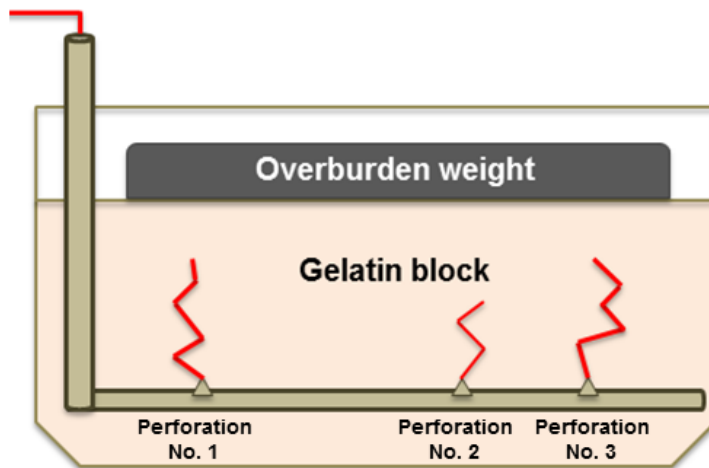
Figure 3.5c – Case III: non-uniform array with the second perforation closer to the last.

3.4   Fracturing Fluids

Dyed glycerin (99.7% concentration) was used as fracturing fluid. The viscosity of pure glycerin is 950 cp. In the preliminary experiments, other fluids have been used. These were dyed water (~1.5 cp) and dyed Vaseline® (~64,000 cp). All viscosity values are given for room temperature and pressure. It was found that as the fracture fluid viscosity increases, from water to glycerin, the number of fractures initiated per given

perforation number increases. This is in agreement with findings in the literature (Wu et al., 2008). However, increasing the viscosity further (exchanging glycerin to Vaseline®) has the opposite effect, leading to less fractures being generated per given perforation number. The reason for the reduced number of fractures is the higher pressure gradients induced in the wellbore when using higher viscosity fluids. It seems that there is an optimal fracturing fluid viscosity at which a maximum number of fractures are generated from a fixed number of perforations.

3.4.1   Pilot Testing

Two –small scale– pilot tests series were performed prior to the actual tests. The main goal of those tests was to establish familiarity with the materials and equipment and make sure that everything works properly. Also, it was intended to use the outcome of those pilot tests to decide which fracturing fluid to use in the actual tests. The two fluids tested were Vaseline® and glycerin.

3.4.1.1   *Vaseline®*

This fluid has very high viscosity (~64,000 cp) at room temperature and must be heated to make it pourable. The test was repeated three times (Figures 3.6a, b and c) on three uniformly spaced perforated wellbores. A slow flow rate of 0.05 mL/min is used for safety purposes, as the highly viscous and compressible fluid can reach high pressures very fast. In all tests one dominant fracture is created from the perforation closer to the vertical section of the wellbore. This can be explained considering the very high pressure gradients in the wellbore induced by the very high viscosity of the fluid. An explanation on how higher viscosity fluids with higher wellbore pressure gradients affect the timing (and sequencing) of fracture initiations in horizontal wells is given in Chapter 4.
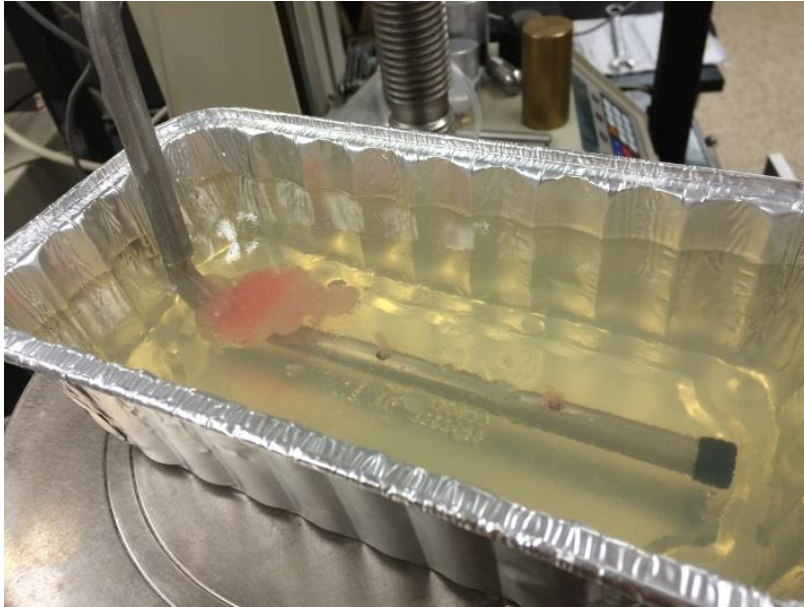
Figure 3.6a – Pilot Test 1 with Vaseline fracturing fluid.
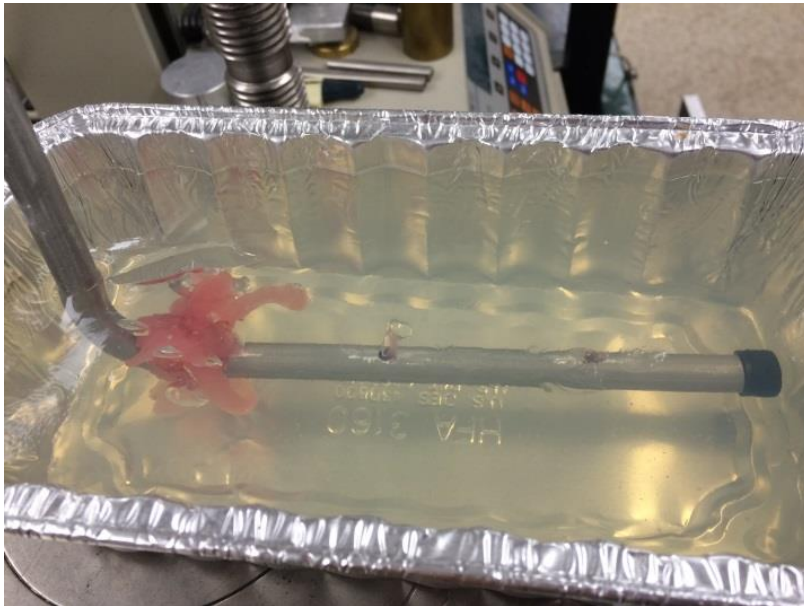
Figure 3.6b – Pilot Test 2 with Vaseline fracturing fluid.
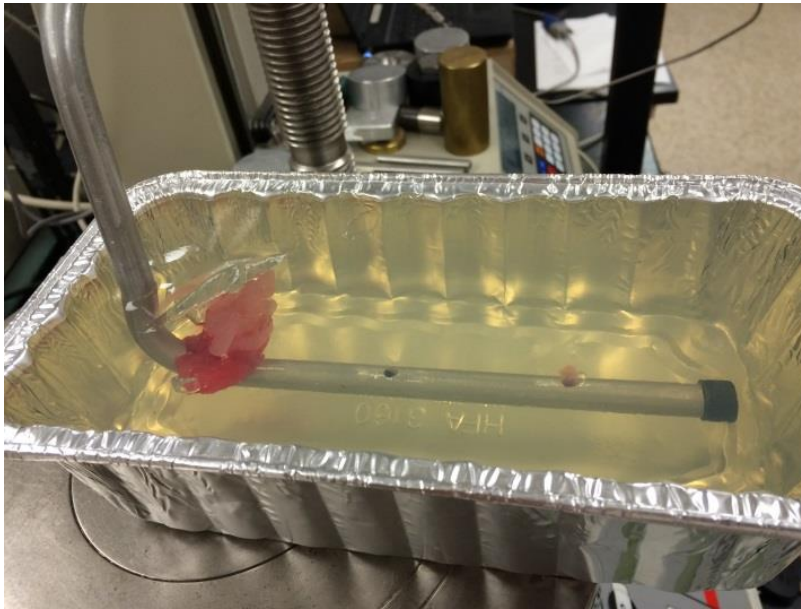
Figure 3.6c – Pilot Test 3 with Vaseline fracturing fluid.

3.4.1.2   Glycerin

This fluid's viscosity (~950 cp) is lower than Vaseline, but still much higher than that of water. Higher flow rates of 50-100 mL/min were used. Tests are made on wellbores with four uniformly spaced perforations. Two perforations generated fractures in these tests; sometimes the two closest to the toe and sometimes the two closest to the heel. It is not clear what determines which of the two perforations will initiate fractures. Figures 3.7a-d are images of one of these tests at various time lapses.

The direction of propagation of the fractures is indicative of the relative magnitude of the principal stresses, as mentioned earlier. Fractures open doing work against the minimum principal stress (Hubbert and Willis, 1957). Figure 3.8 shows an image captured from an angle almost parallel to the wellbore enabling accurate inspection of the induced fractures. Within some margin, the fractures open against the longer horizontal dimension $-y-$ making it the direction of the least principal stress. The plastic container is more flexible along the longer horizontal dimension $-y-$ compared to the shorter $-x-$ likely making it the direction of S_3. The reason for the margin is the presence of the container's walls, acting as boundaries affecting fracture growth.
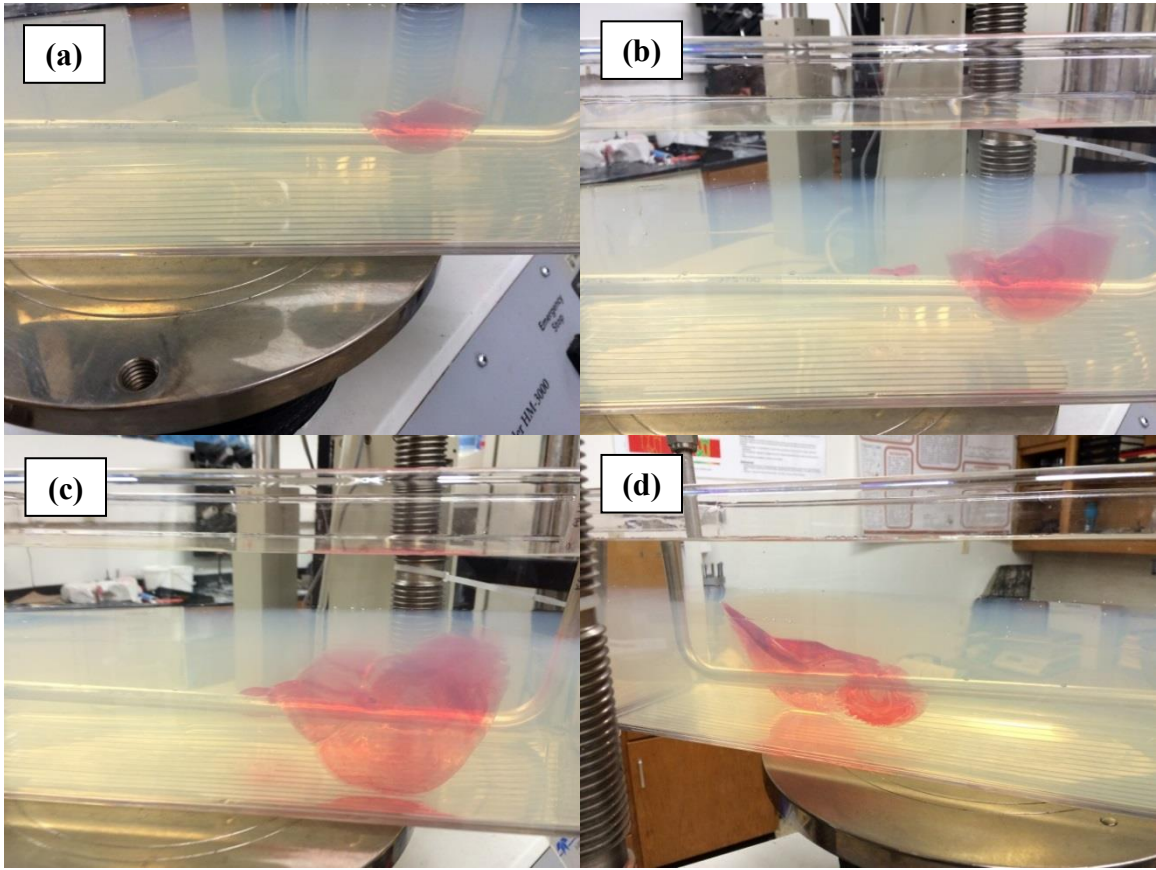
Figure 3.7 – Pilot test with glycerin fracturing fluid. The images are arranged from (a) to (d) with respect to the time captured.
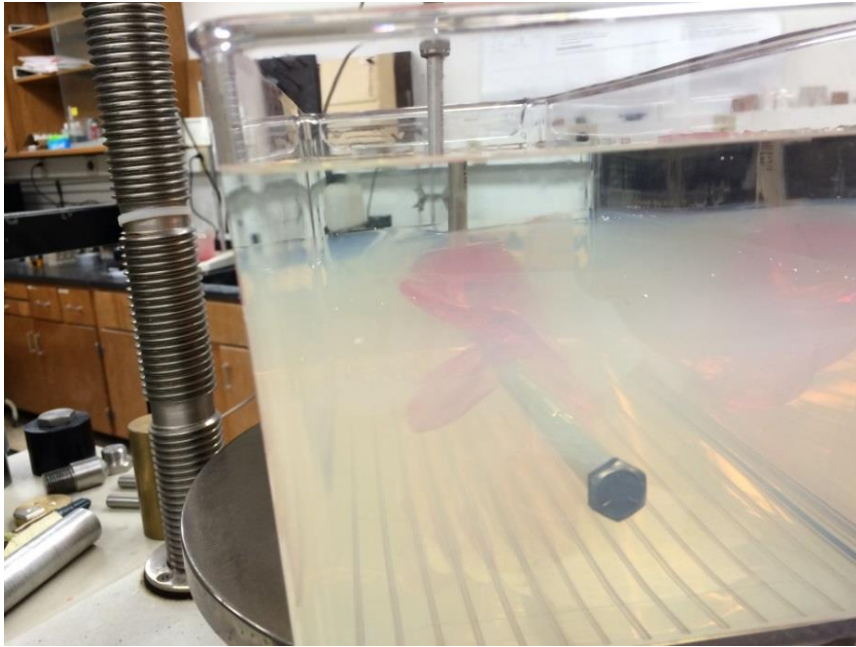
Figure 3.8 – Image taken parallel to wellbore. Fracture opening direction indicates S$_3$ to be oriented perpendicular to the wellbore in the horizontal direction.

Table 3.2 summarizes the properties of the three different fracturing fluids; water, glycerin and Vaseline. The results of the pilot tests have shown that glycerin usability as fracturing fluid for the purposes of the experimental program is far superior to Vaseline. The major factor in the decision was glycerin's ability to generate multiple fractures from one horizontal wellbore. Furthermore, the relatively lower viscosity of glycerin, compared to Vaseline, makes laboratory-to-field scaling (de Pater, 1994) easier, since it is closer to the viscosity of fracturing fluids used in field conditions.

Table 3.2 – Properties of the fracturing fluids used in the tests.

Fluid	Approximate viscosity (cp)	Compressibility (10^{-6}psi^{-1})	Gradients generated in wellbore during pumping	Ability to initiate multiple fractures
Water	1.5	3.2	low	✘
Glycerin	950	1.6	medium	✓
Vaseline®	64,000	Very low	high	✘

3.4.2 Injection Flow Rates

Results from pilot testing performed with dyed glycerin fracturing fluid, as well as findings in the literature, from other studies using similar specimen material and fracturing fluid (Wu et al., 2008) were considered for choosing the injection flow rate used in the tests. It was decided to use 100 mL/min, as this rate is high enough to generate multiple fractures, but not too high that the fractures propagate so fast, that reach the specimen surface, before other fractures are produced. To ensure reliable comparison, the same injection flow rate was used in every test.

3.5   Multiple Fracture Homogeneity Quantification Method

The parameter used for quantification of fracture homogeneity is the fracture length (equal to half-length in the case of bi-wing fractures). The length of each generated fracture can be normalized by the length of the longest fracture produced in the corresponding test as shown in Equation 3.1,

$$N_i^{length} = \frac{l_i}{l_{max}} \qquad (3.1)$$

where N_i^{length} is the normalized length of the ith fracture, l_i is the actual length of that particular fracture and l_{max} is the length of the longest fracture generated. Consistent units should be used in the numerator and the denominator producing a dimensionless quantity.

For each experimental test, the sum of the normalized lengths of the fractures generated is calculated and then divided by the total number of perforations using Equation 3.2,

$$FLHF = \frac{1}{n} \sum_1^n N_i^{length} \qquad (3.2)$$

where the value of i varies from 1 to n, the total number of fractures expected to be generated in each test, which is equal to the number of perforations. We refer to this value as the fracture length homogeneity factor (*FLHF*) and it can vary from zero to one depending on the degree of homogeneity of fracture growth. Fully homogeneous multiple fracture growth, where all fractures have the same length will give a value of one, while heterogeneous growth yields values closer to zero.

The *FLHF* is then plotted against the independent variable which for three perforation cluster arrays is the normalized position of Perforation No. 2 ($N_2^{position}$) and is calculated using Equation 3.3,

$$N_2^{position} = \frac{D_1^2}{D_1^3} \tag{3.3}$$

where D_1^2 is the distance between Perforations No. 2 and No. 1 and D_1^3 is the distance between Perforations No. 3 and No. 1. The units of both must be the same. Similarly, $N_1^{position}$ and $N_3^{position}$ will be zero and one respectively.

Table 1.1 presents synthetic data from five example cases of three perforation arrays, similar to the ones used in the actual experimental program:

- Example 1: uniform perforation spacing
- Example 2 High/Low homogeneity: middle perforation closer to the heel of the horizontal wellbore with homogeneous/non-homogeneous fracture growth
- Example 3 High/Low homogeneity: middle perforation closer to the toe of the horizontal wellbore with homogeneous/non-homogeneous fracture growth

The quantities of $l_{1,2\ and\ 3}$ and $D_1^{1,2\ and\ 3}$ tabulated are assumed to be in consistent units.

Table 3.3 – Hypothetical data for the example cases.

Parameters for example	1	2 High homogeneity	2 Low homogeneity	3 High homogeneity	3 Low homogeneity
$l_1\ (in)$	3	3	2	3	7/2
$l_2\ (in)$	1	5/2	1	12/5	1
$l_3\ (in)$	3	7/2	4	14/5	2
N_1^{length}	1	6/7	1/2	1	1
N_2^{length}	1/3	5/7	1/4	4/5	2/7
N_3^{length}	1	1	1	1	4/7
$D_1^1\ (in)$	0	0	0	0	0
$D_1^2\ (in)$	7/2	2	2	5	5
$D_1^3\ (in)$	7	7	7	7	7
$N_1^{position}$	0	0	0	0	0
$N_2^{position}$	1/2	2/7	2/7	5/7	5/7
$N_3^{position}$	1	1	1	1	1
FLHF	7/9	6/7	4/7	41/45	5/8

Using the results a multiple fracture length profile plot (Figure 3.9) can be generated for each example case, in which a perfectly homogeneous growth case yields a straight line at fracture normalized length of one. Moreover, a fracture growth homogeneity by length versus $N_2^{position}$ plot (the rows in the red dotted boxes) is generated using the calculated *FLHF* as shown in Figure 3.10; the perforation spacing case which generates the higher *FLHF* is the best.
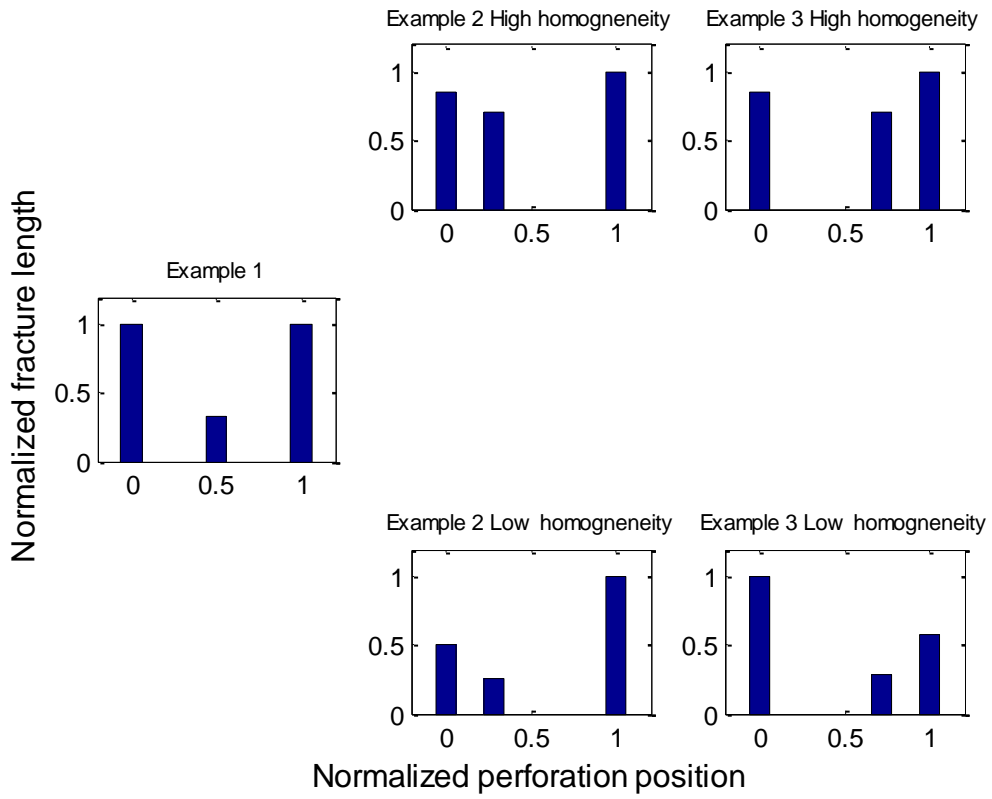
Figure 3.9 – Fracture growth profiles for the example cases.
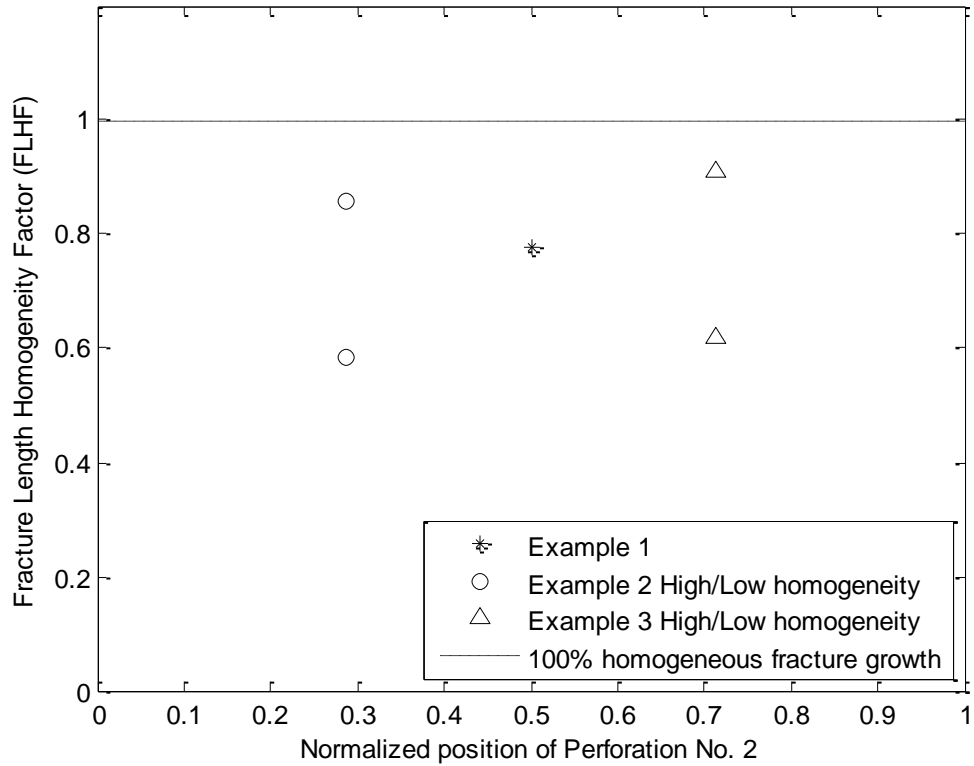
Figure 3.10 – Fracture growth homogeneity plots for the example cases.

The closer the points are to the dotted line, the more homogeneous the fracture growth is. This technique is used to quantify the degree of homogeneity in our experiments and prove, or disprove the hypothesis tested. This method is applicable in field-scale as it is for laboratory-scale cases when information on fracture length is available, for example by microseismic data. *FLHF* can also be calculated and assessed at various time intervals during a fracture stimulation job.

Chapter 4

Results and Discussion

This chapter presents the results of the experimental tests and discusses what they indicate in relation to the pre-stated hypothesis. Photographic snapshots taken during each test are provided along with the data acquisition of key parameters. Then a fracture growth homogeneity analysis is performed to quantify the fracture length homogeneity achieved in each test and the extent to which the results agree with numerical simulations and field data is assessed.

4.1   Key Observations

Most of the tests exhibited a pressure profile similar to that shown in Figure 4.1, which is close to the behavior predicted in Figure 2.5. Pressure increases rapidly, until it reaches the highest point, which sometimes becomes a small plateau at the fracture initiation pressure.

Interestingly, despite having multiple fracture generation, only one peak in pressure is observed. This can be attributed to the lower compressibility of glycerin, which is 1.6×10^{-6} psi^{-1} compared to 3.2×10^{-6} psi^{-1} for water. Low compressibility hinders fluid displacement during pressure increase. For the same pressure increase, the fluid with the lower compressibility experiences lower change in volume, compared to the fluid with higher compressibility. This smaler volumetric compression during pressure increase compared to water does not allow glycerin to expand in the wellbore, as much as it would if it was water which is almost incompressible.

Another observation is that in all tests the fluid is lagging the crack tip, as the fractures grow; glycerin is almost never present at the crack tip. The fluid at the crack tip is almost always air (see Figure 4.2). This has to do with the viscosity of the fracturing

fluid used. The viscosity of glycerin is too high to penetrate to the fracture tip and air becomes the fluid causing the breakdown when a fracture is generated. This situation is known as dry tip (Groenenboom et al., 1999). How far in the fracture glycerin reaches is determined by capillary forces related to fracture geometry (opening) and the two fluids present in the fracture. Finally, all tests end with one fracture dominating, by propagating much faster than the rest breaking to the surface of the specimen.
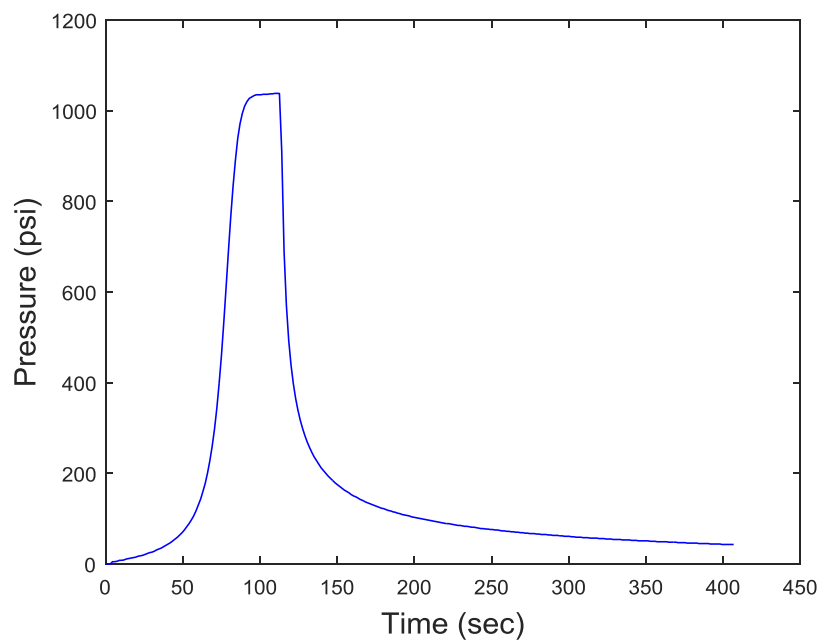
Figure 4.1 – Generic pressure behavior observed during the tests.

Figure 4.2 – Fracture growth with the air previously present in the wellbore at the crack tip, followed by glycerin fracturing fluid. Inside the dotted box, we see the dry tip of the fracture.

44

4.2   Experimental Results

4.2.1   Case I

In this series of tests, the spacing between the three perforations is equal at 3.5 inches. Case I is intended to be the uniform perforation distribution base case in the testing of our hypothesis. Three tests were performed for this case.

Figure 4.3 – Perforation configuration schematic for Case I.

4.2.1.1   Test 1

Figure 4.4
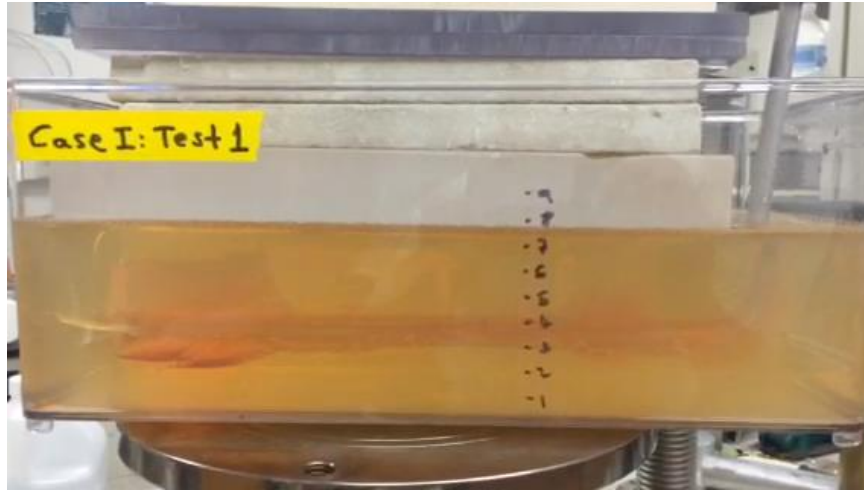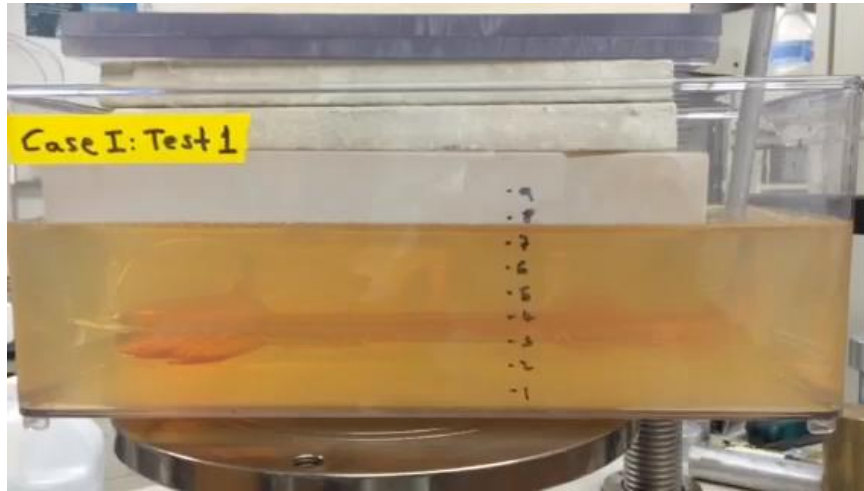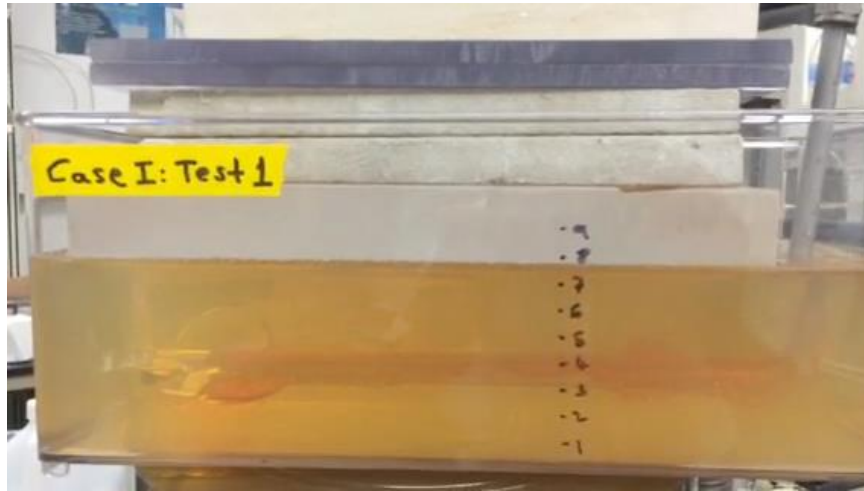
Figure 4.4 – Snapshots from Case I Test 1.
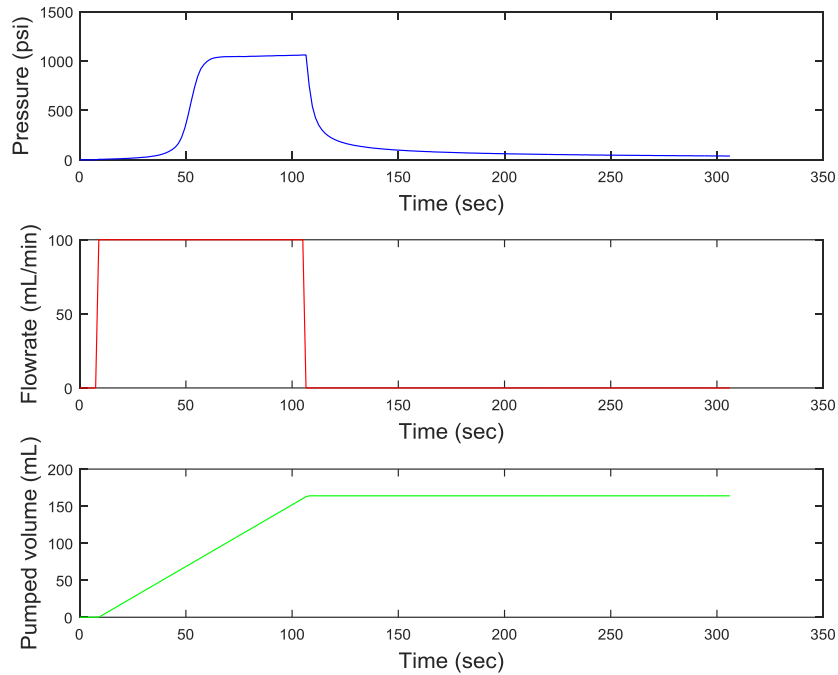
Figure 4.5 – Pump pressure, flow rate and volume variation during Case I Test 1.

In Case I Test 1, the first fracture was initiated from the first perforation. Then fluid moved along the length of the wellbore passing the second perforation generating small fractures around the wellbore. Eventually the third perforation initiated two fractures; a smaller horizontal one longitudinally to the wellbore and a bigger vertical one also longitudinal to the wellbore, opening against the specimen width. This bigger fracture generated from the third perforation was the one that first reached the surface of the gelatin sample. Notably, while the fracture from the first perforation stopped propagating, the fractures generated from the third perforation were still propagating.

4.2.1.2   Test 2

Figure 4.6
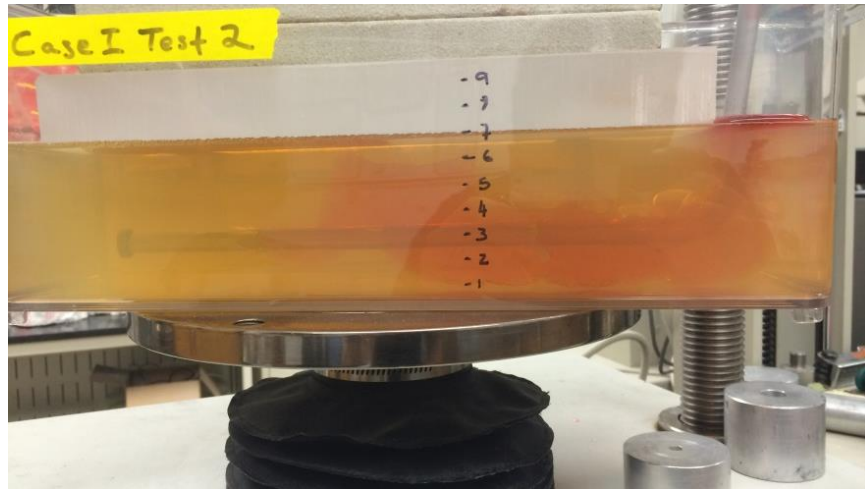
Figure 4.6 – Snapshots from Case I Test 2.
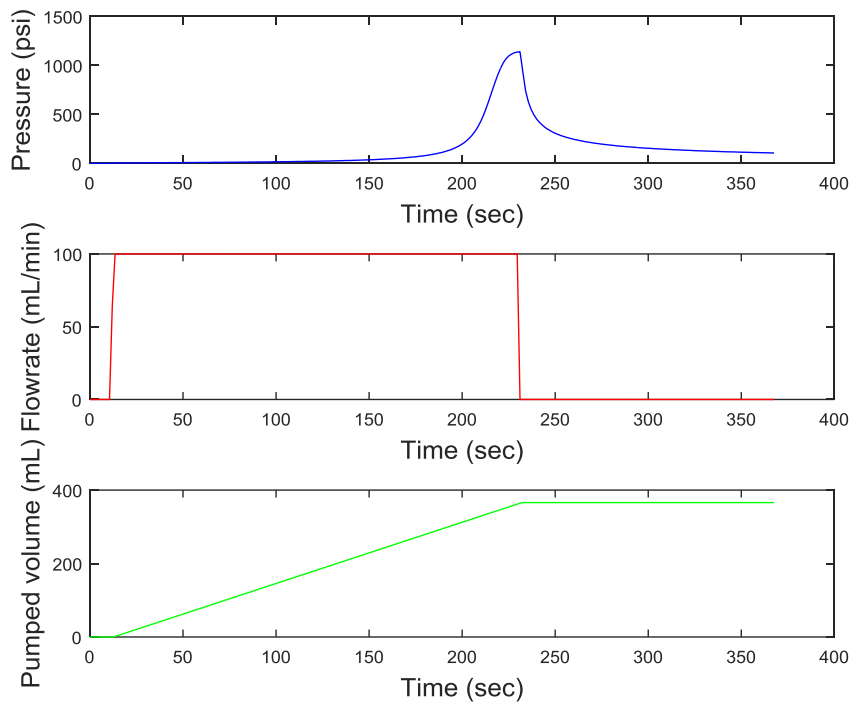
Figure 4.7 – Pump pressure, flow rate and volume variation during Case I Test 2.

Case I Test 2 generated a total of three fractures as in Case I Test 1. The first fracture initiated at the middle perforation and then another one was initiated next to it towards the heel of the lateral. Finally, a third fracture was initiated from the first

perforation and all three fractures grew quite homogeneously in length. Small fractures, created along the deviated and vertical parts of the wellbore let fluid reach the surface. This may be possibly due to poor bonding between the wellbore and the gelatin sample.

4.2.1.3   Test 3
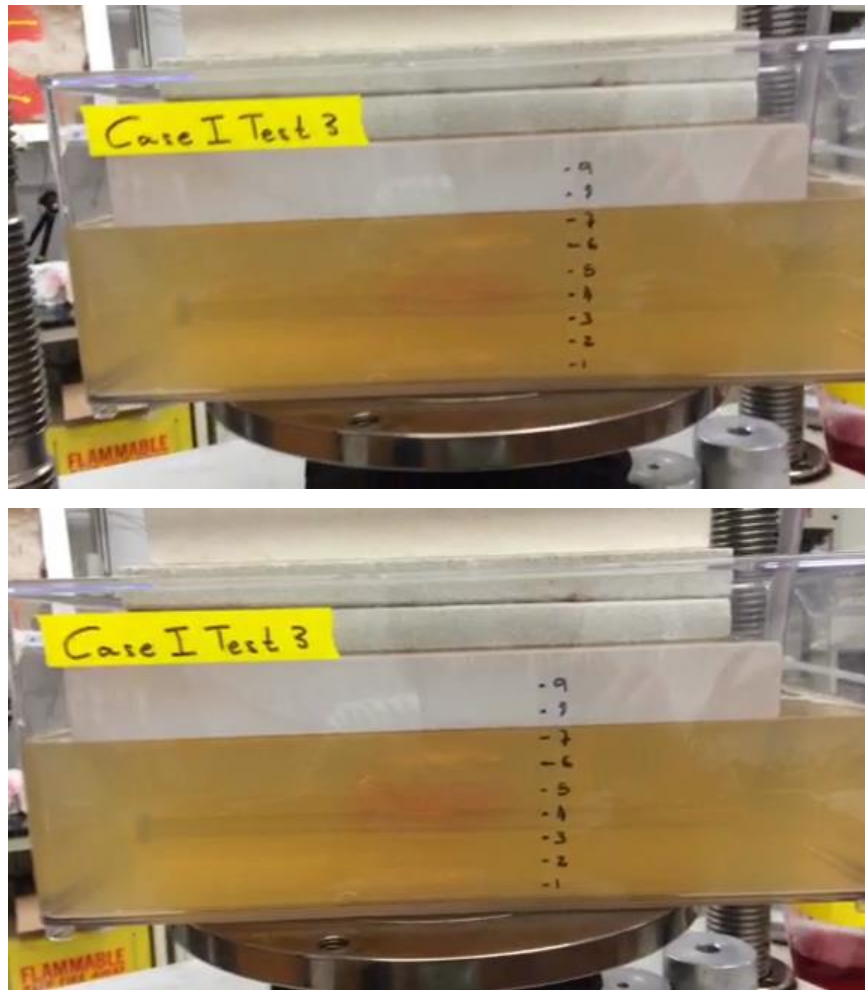
Figure 4.8

Figure 4.8 – Snapshots from Case I Test 3.

Figure 4.9 – Pump pressure, flow rate and volume variation during Case I Test 3.

In Case I Test 3, only one fracture was produced, initiated from the middle perforation. It is clearly visible from the snapshots that the compressed air is present at the tip of the fracture followed by dyed glycerin.

4.2.2 Case II

For Case II Perforation No. 2 is moved closer to the heel of the horizontal wellbore compared to Case I. The distance between Perforations No. 1 and No. 2 is 2 inches and the distance between Perforation No. 2 and No. 3 is 5 inches.
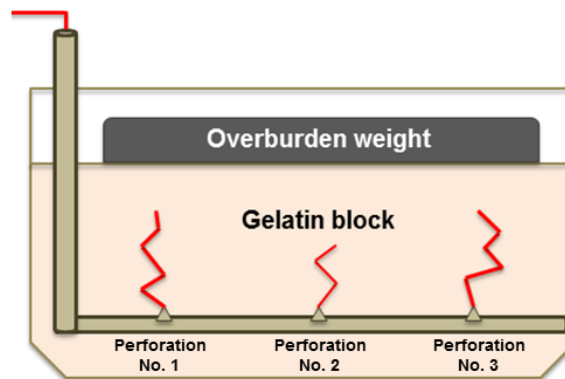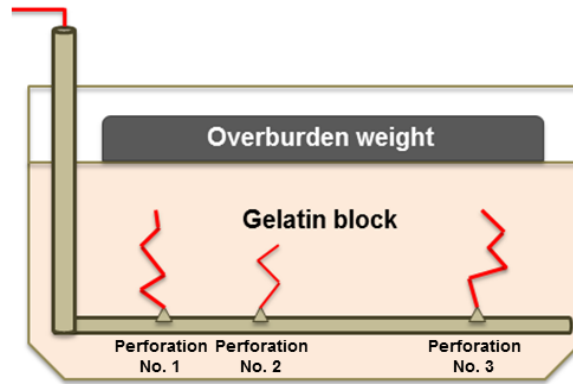

Figure 4.10 – Perforation configuration schematic for Case II.

4.2.2.1 Test 1
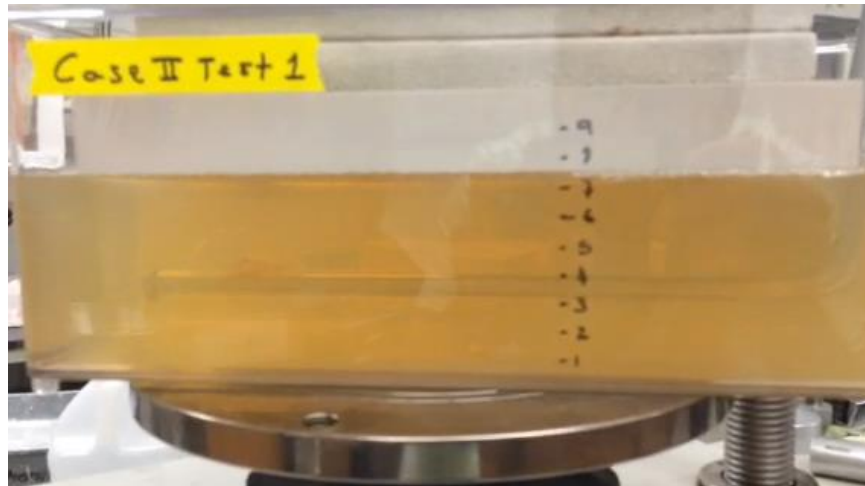
Figure 4.11
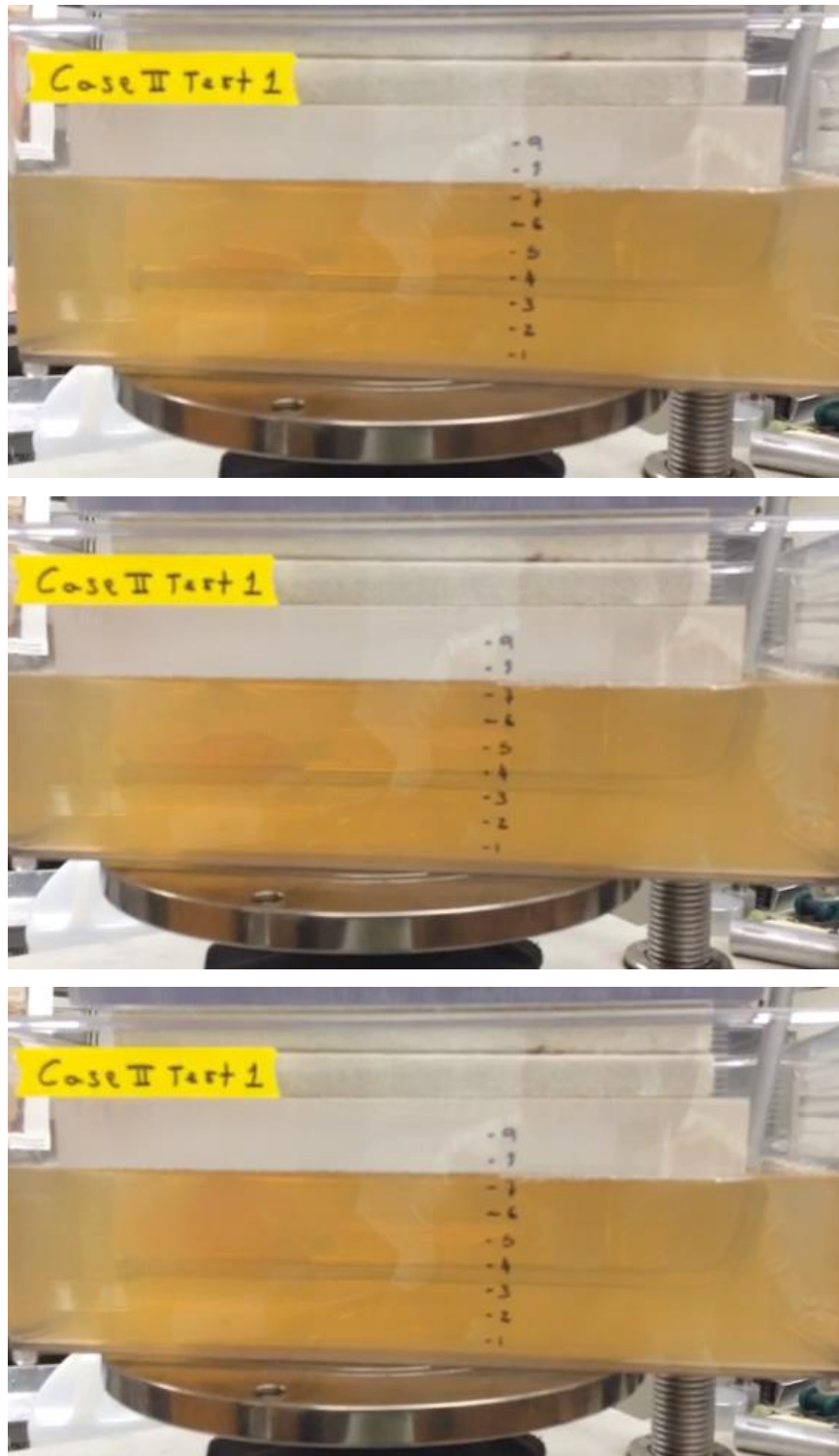
Figure 4.11 – Snapshots from Case II Test 1.

Figure 4.12 – Pump pressure, flow rate and volume variation during Case II Test 1.

Case II Test 1 produced only one fracture from the third perforation, which is nearest to the toe of the well. The first two perforations did not generate any fracture despite being nearer to the heel of the wellbore, where the fluid pressure is higher, due to friction between the fluid and the internal surface of the wellbore. Moreover, the geometry of the fracture formed was very close to radial (a vertical fracture longitudinal to the wellbore with equal height and length).

4.2.2.2   Test 2

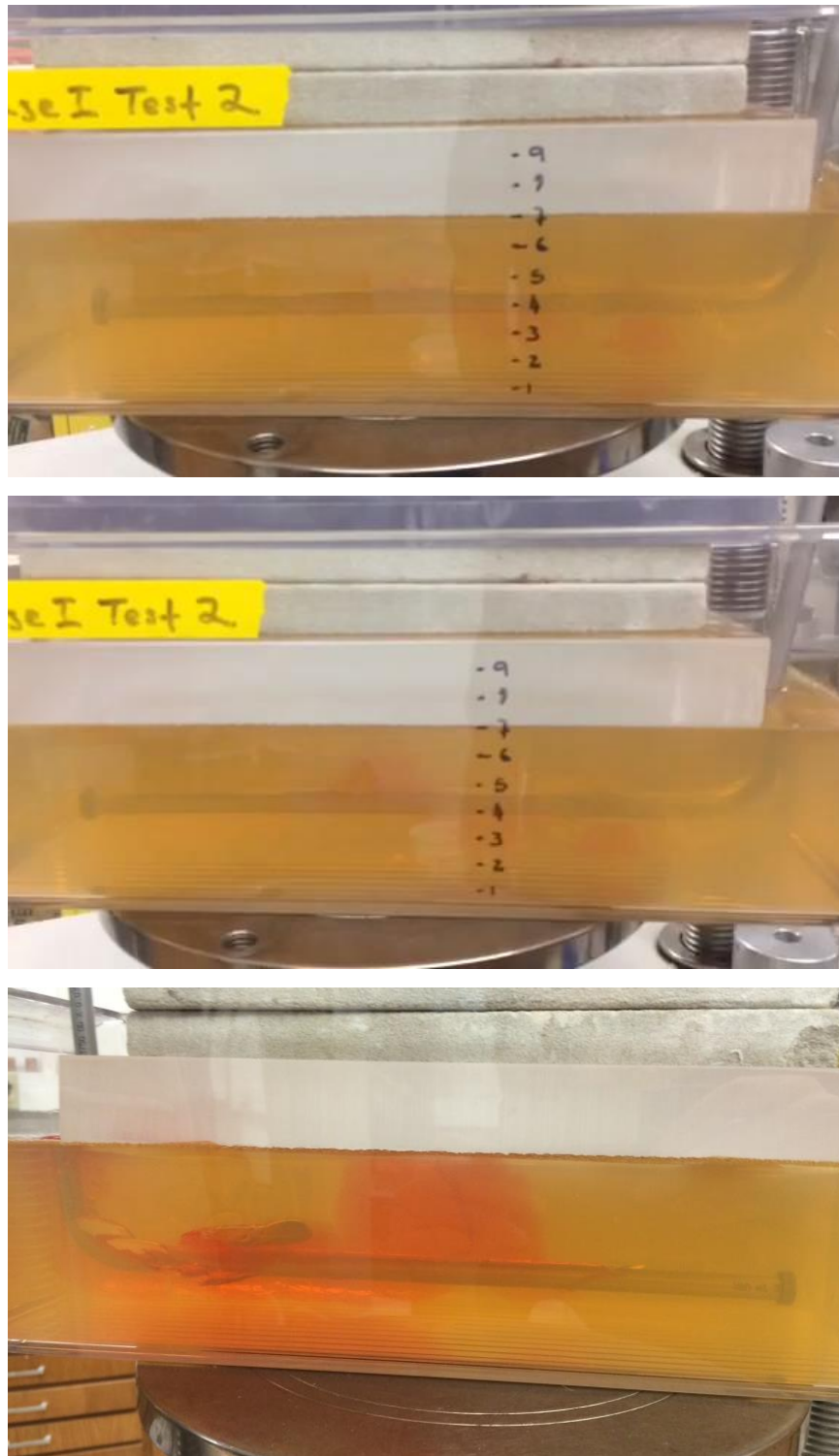**Figure 4.13**
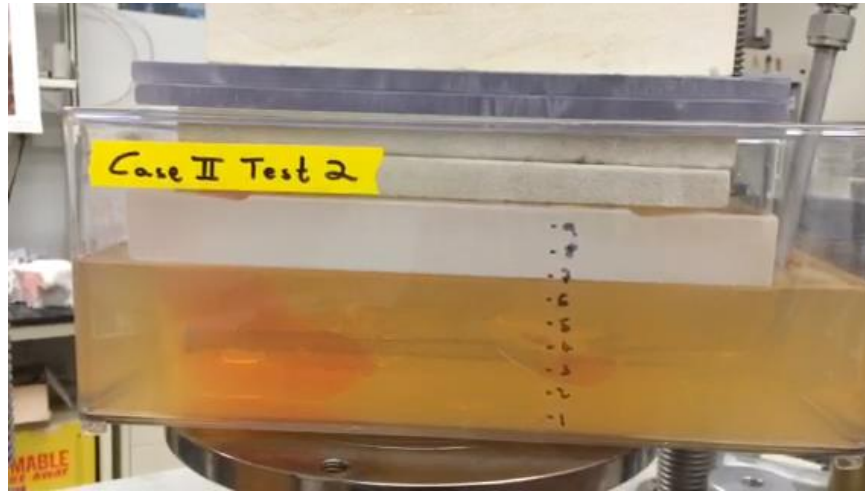
Figure 4.13 – Snapshots from Case II Test 2.
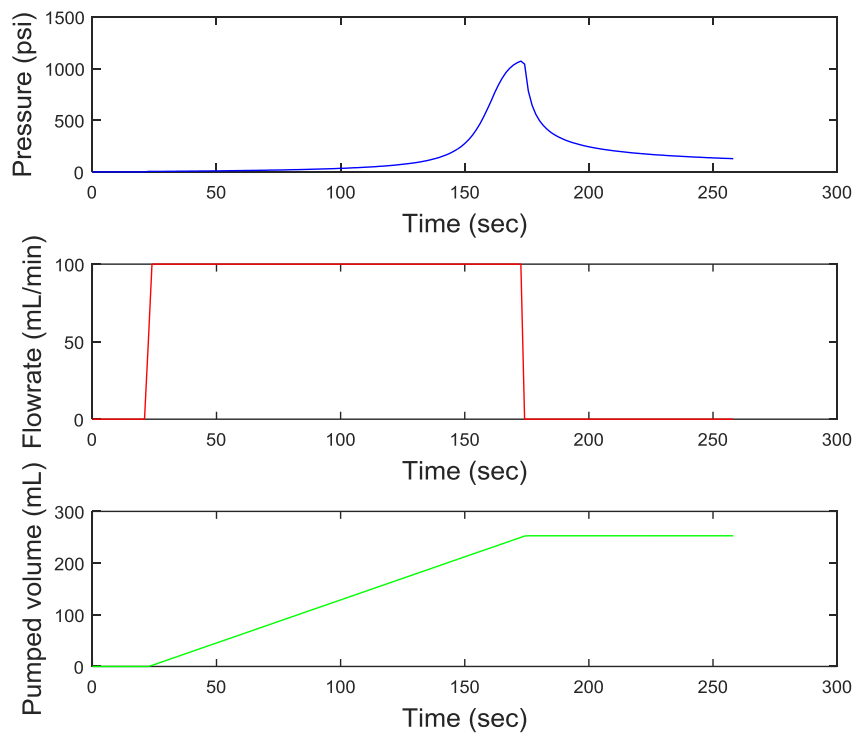
Figure 4.14 – Pump pressure, flow rate and volume variation during Case II Test 2.

Two fractures were produced in Case II Test 2. The first fracture was generated from the first perforation (near the heel of the well). As this first fracture was

propagating, the second one was initiated from the third perforation closer to the toe and began growing much faster than the first fracture. Eventually, the second fracture reached the surface of the specimen.

4.2.2.3 Test 3
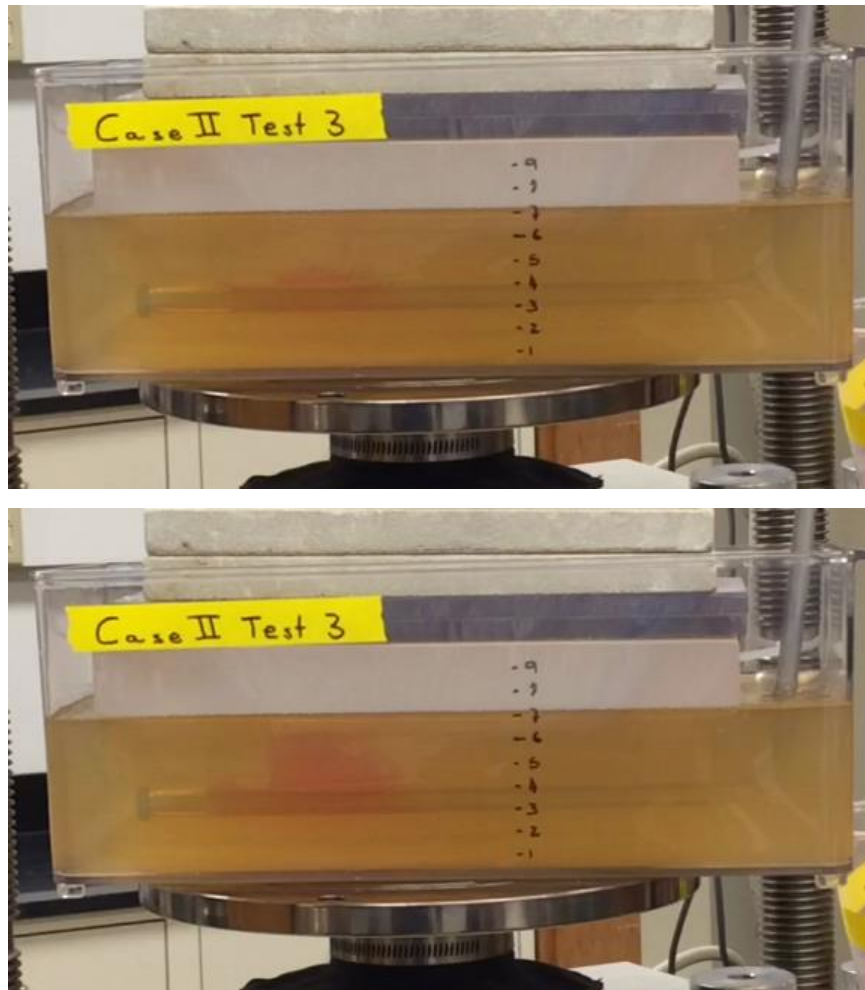
Figure 4.15
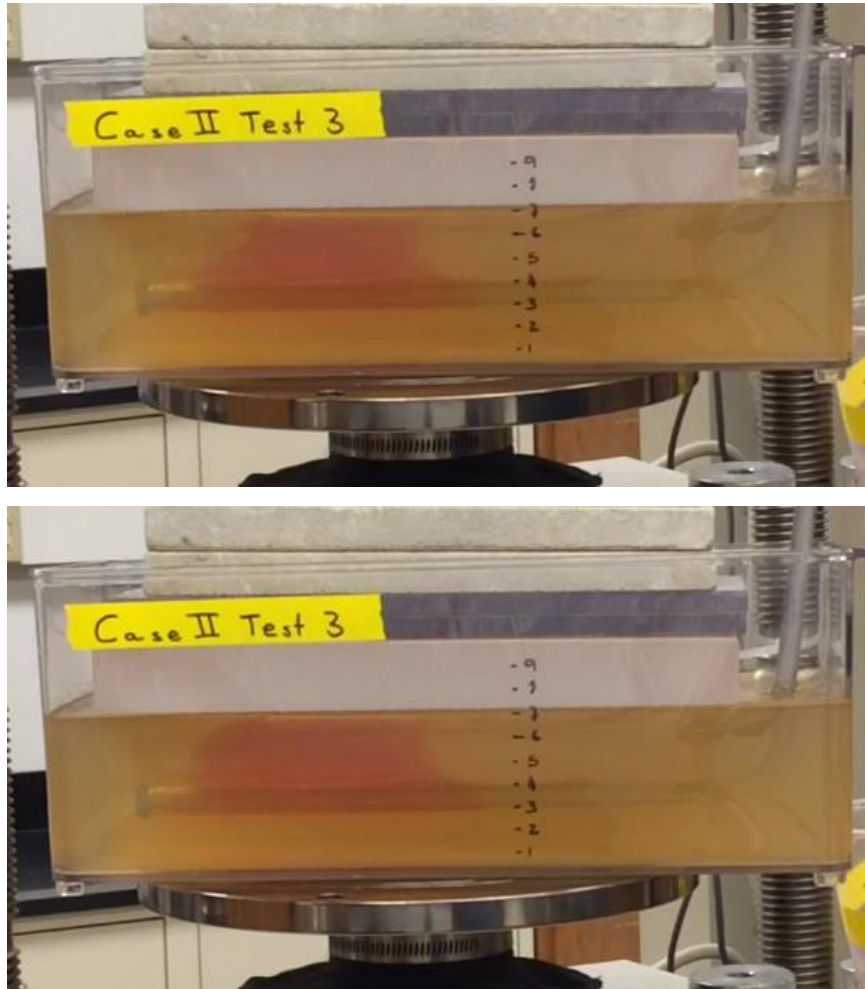
Figure 4.15 – Snapshots from Case II Test 3.
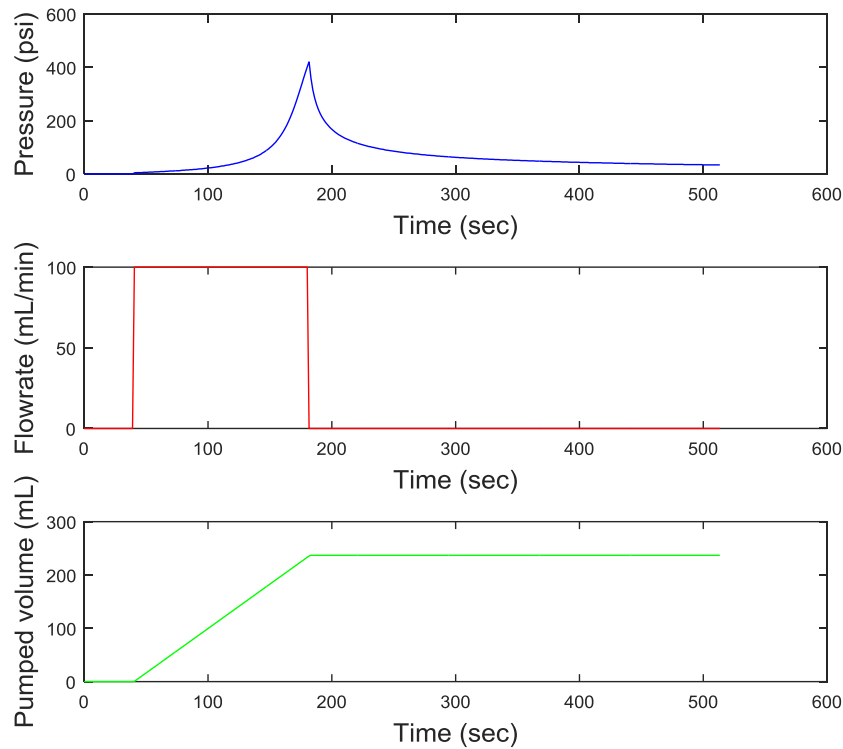
Figure 4.16 – Pump pressure, flow rate and volume variation during Case II Test 3.

A single vertical fracture was produced in Case II Test 3 from Perforation No. 3. It propagated upwards from the horizontal lateral and extended a long distance along the length of the wellbore, without reaching Perforation No. 2. This was one of the two tests that gave maximum pressure recording considerably less than the rest of the tests; the other one being Case III Test 3 shown later.

4.2.3 Case III

For Case III Perforation No. 2 is moved closer to the toe of the horizontal wellbore compared to Cases I and II. The distance between Perforations No. 1 and No. 2 is 5 inches and the distance between Perforation No. 2 and No. 3 is 2 inches.
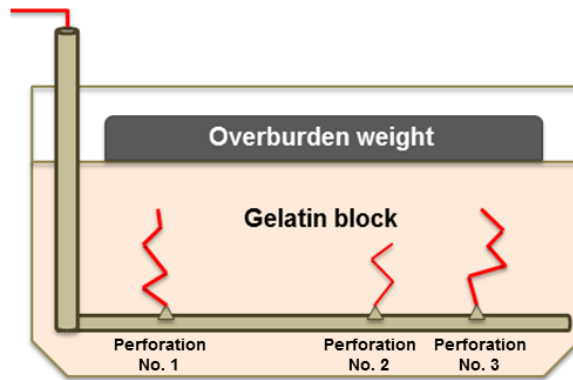
Figure 4.17 – Perforation configuration schematic for Case III.

4.2.3.1   Test 1

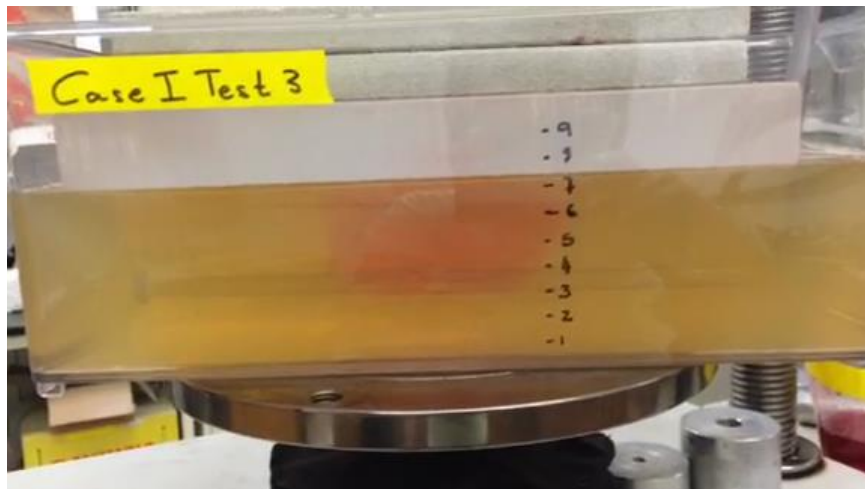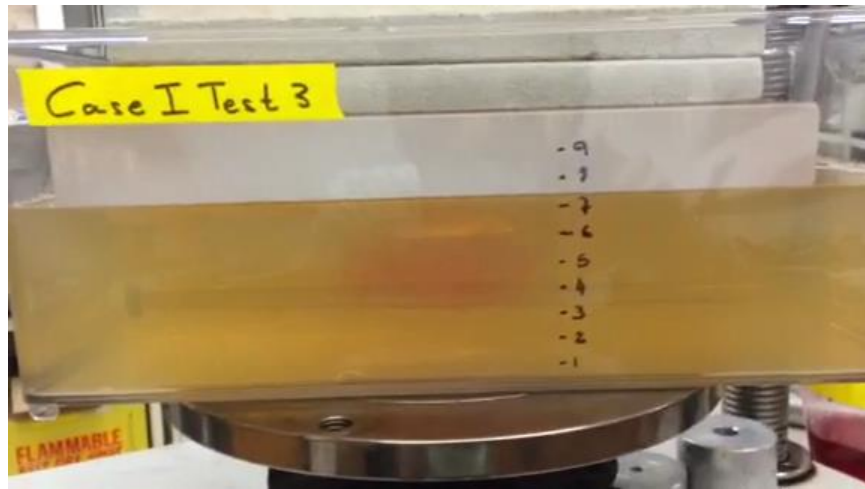**Figure 4.18**

Figure 4.18 – Snapshots from Case III Test 1.
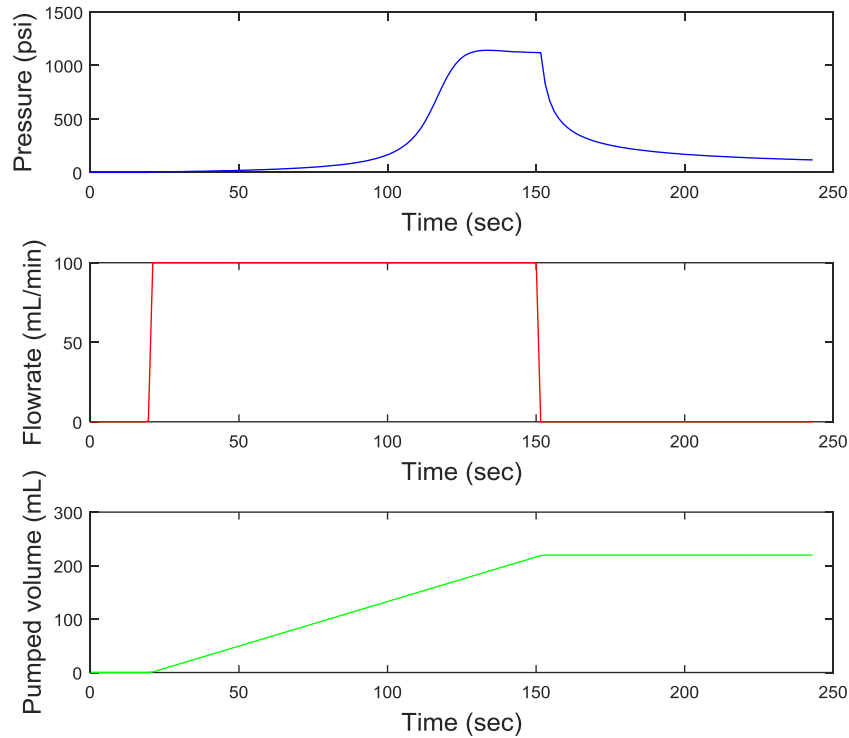
Figure 4.19 – Pump pressure, flow rate and volume variation during Case III Test 1.

Case III Test 1 produced three fractures, one from each perforation. The first two fractures were initiated almost simultaneously from the second and third perforation. A few seconds later a third perforation was initiated from the first perforation. The last fracture continued to grow, both in length and also longitudinally along the deviated and vertical part of the wellbore, eventually reaching the surface. Interestingly, the fractures form the second and third perforations were not fully longitudinal to the wellbore as in other cases.

4.2.3.2 Test 2
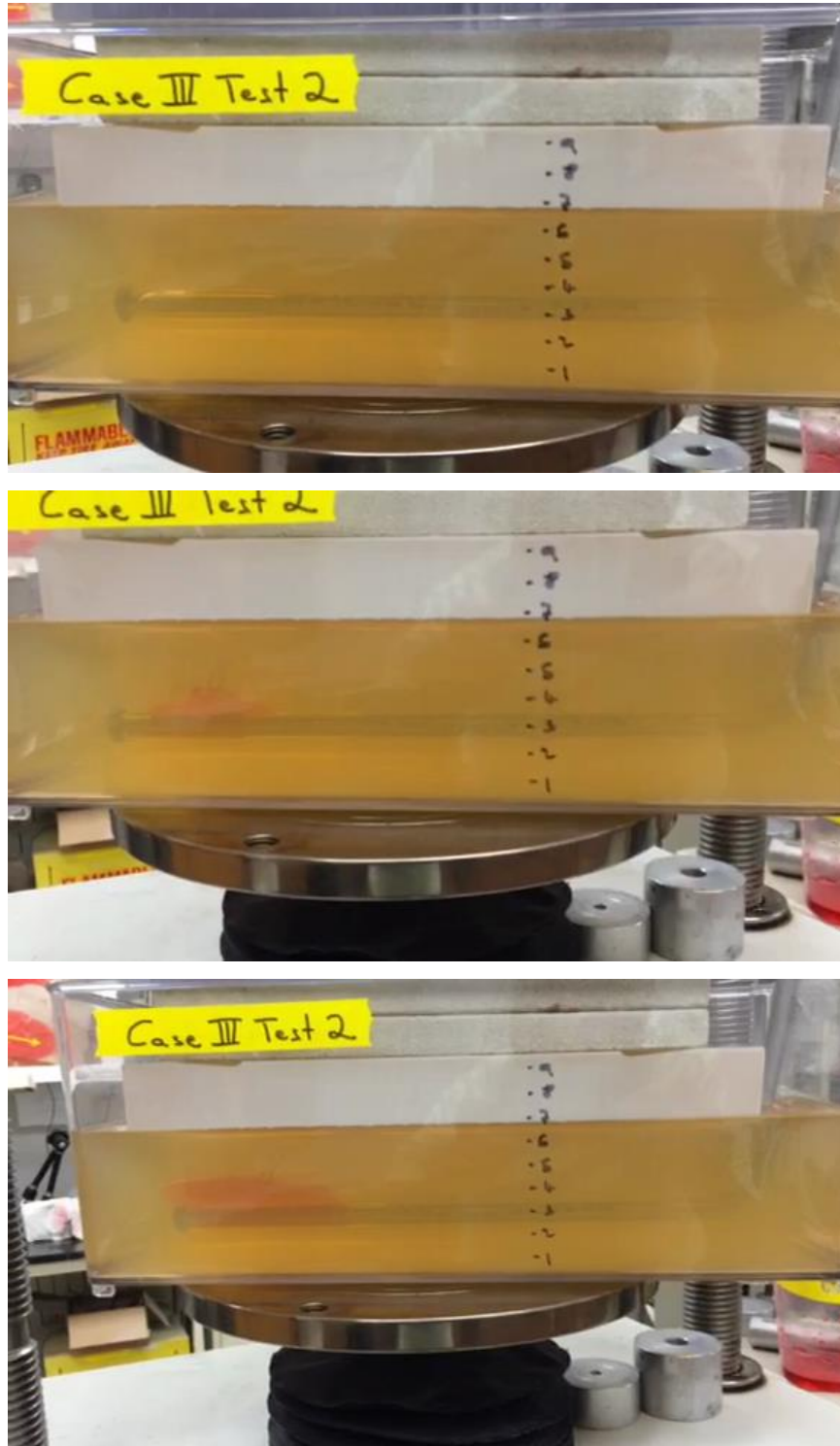
Figure 4.20
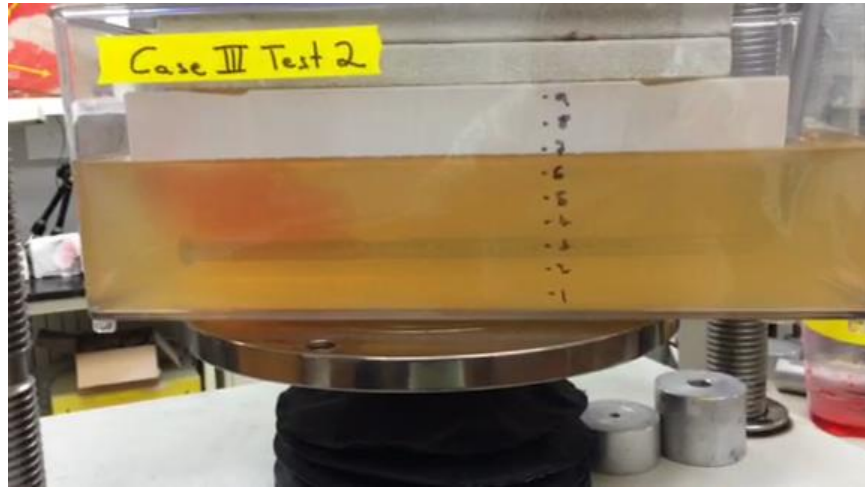
Figure 4.20 – Snapshots from Case III Test 2.
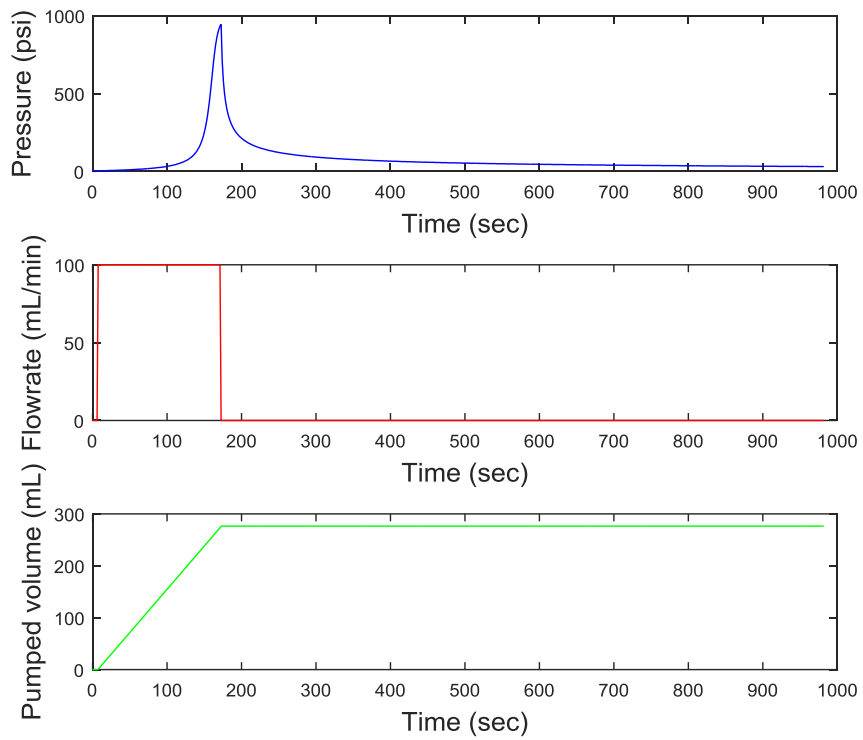
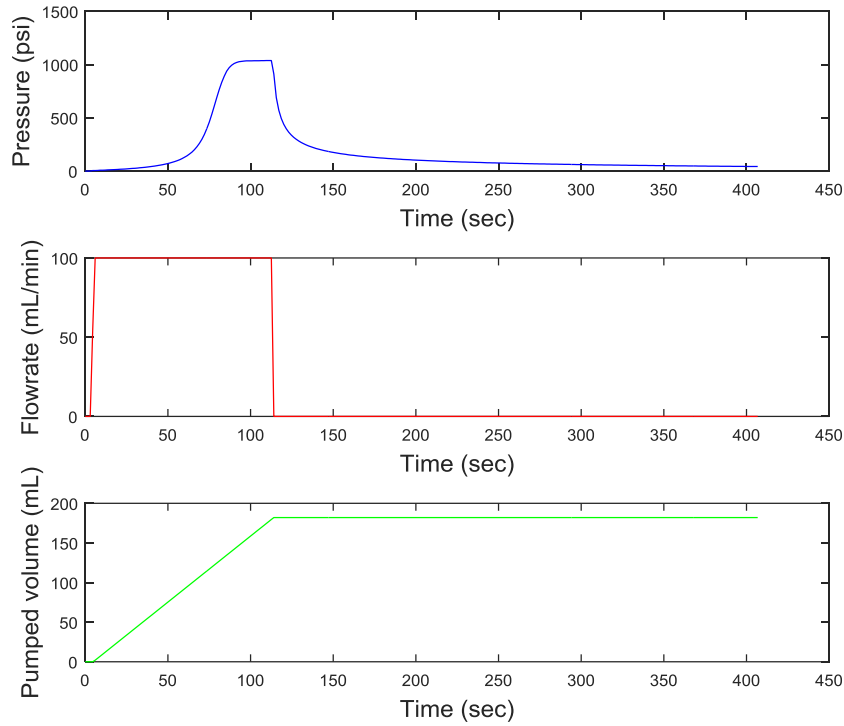**Figure 4.21 – Pump pressure, flow rate and volume variation during Case III Test 2.**

In Case III Test 2 only one fracture was produced and was initiated from the third perforation. This fracture was longitudinal to the wellbore growing vertically in length, eventually cracking the surface of the specimen.

### 4.2.3.3   Test 3

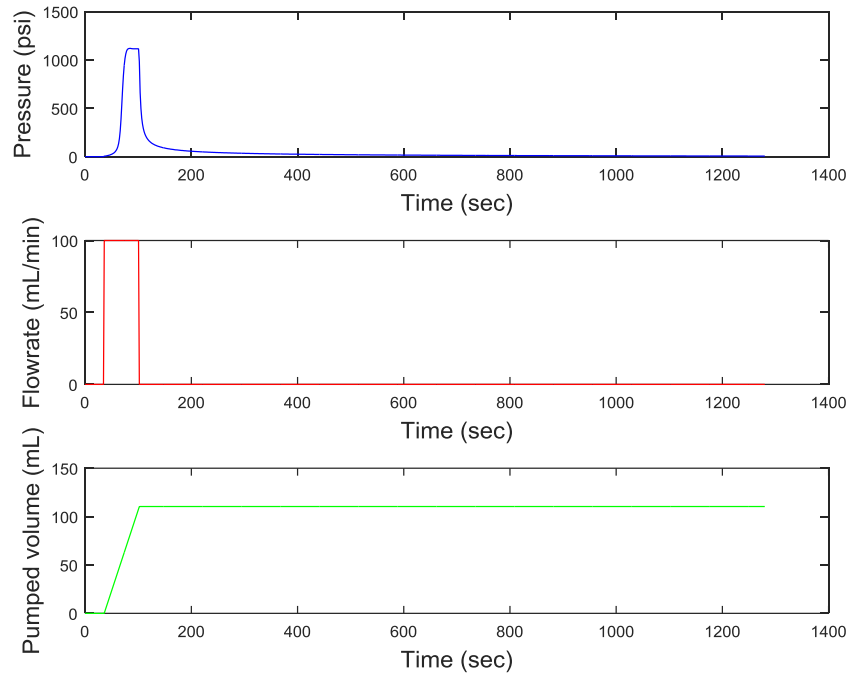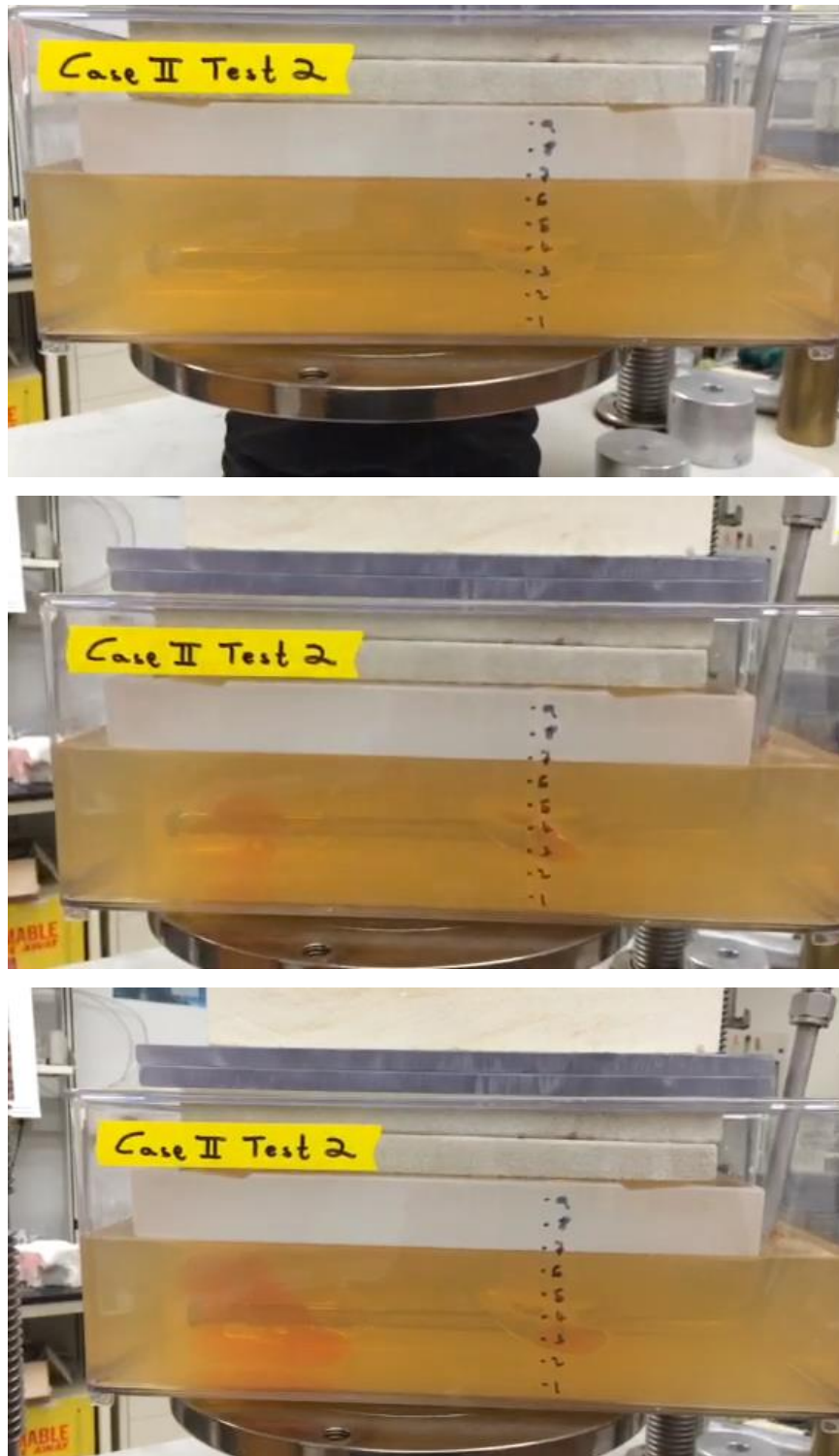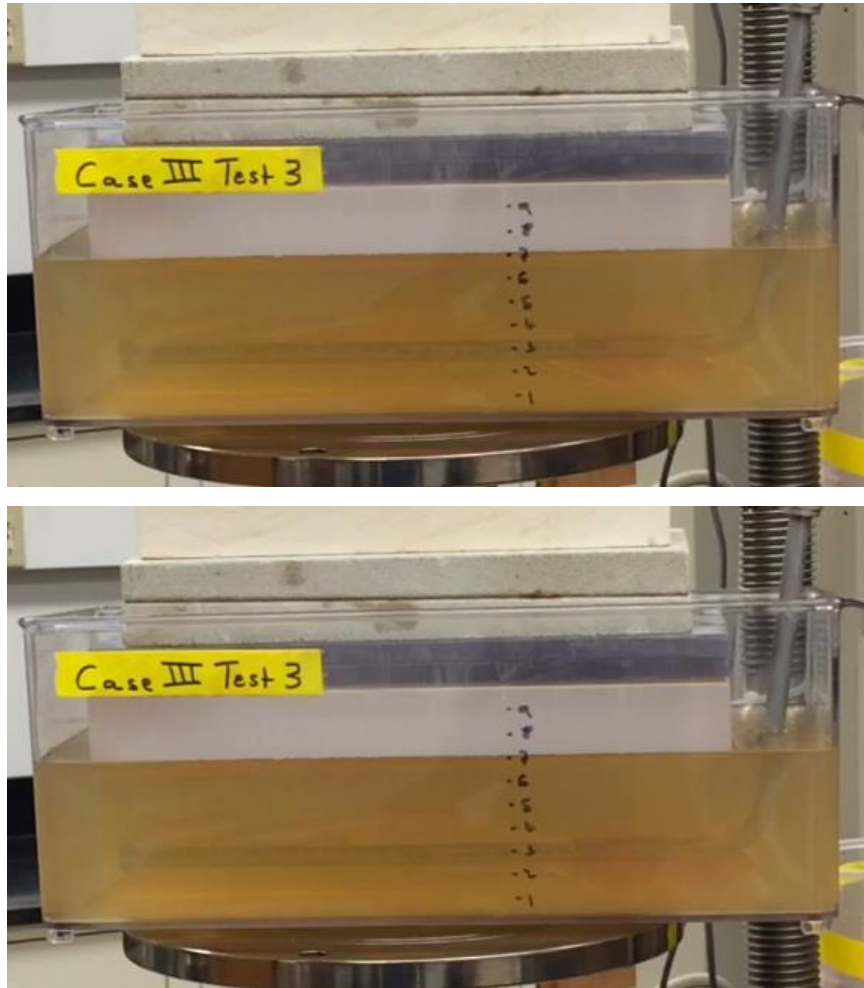**Figure 4.22**
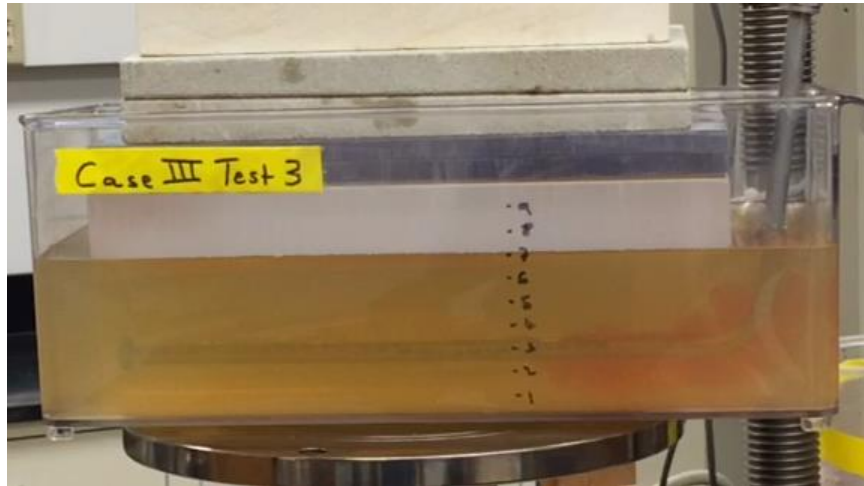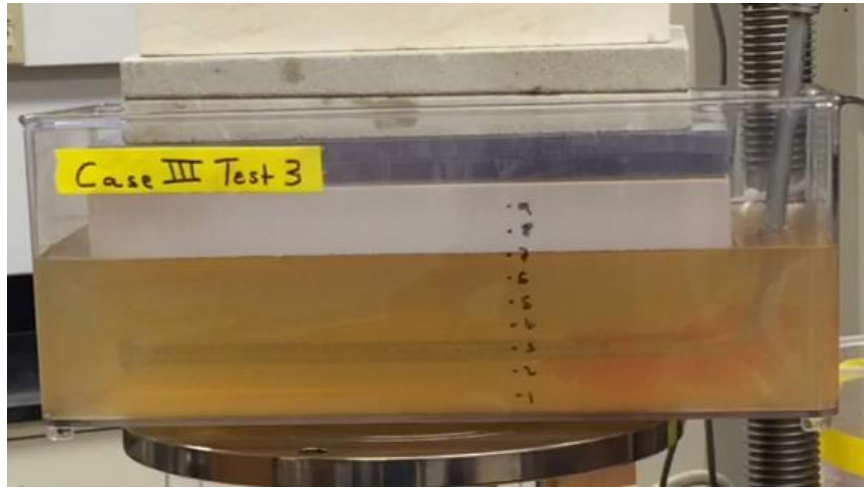
Figure 4.22 – Snapshots from Case III Test 3.
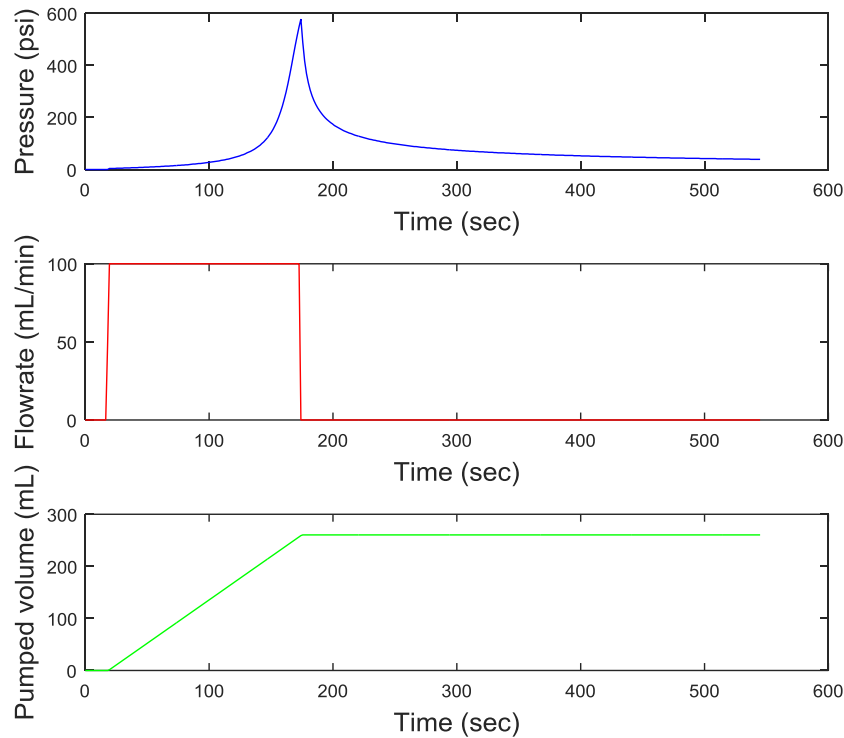
Figure 4.23 – Pump pressure, flow rate and volume variation during Case III Test 3.

Case III Test 3 generated one fracture from Perforation No. 1, propagating longitudinally above and below the wellbore. The fracture extended along the deviated part of the wellbore and cracked the surface of the specimen next to the overburden weight, spilling out fracturing fluid. The maximum pressure reached in this test was, similar to Case II Test 3, significantly lower than the rest of the tests.

4.2.4   Summary of Results

Table 4.1 provides a summary of the results of all tests. Every test led to generation of fracture(s). The materials, concentrations and stress conditions for all the tests were kept constant to ensure result reliability. Moreover, the same injection flow rate (100 mL/min) was used in all nine tests.

68

Table 4.1 – Test conditions and results summary (0.2 psi overburden pressure).

Experiment	Maximum pressure recorded (psi)	Number of fractures generated	Perforation initiating first fracture
Case I Test 1	1061	3 (2 from Perf. No. 2)	No. 1
Case I Test 2	1139	3 (2 from Perf. No. 2)	No. 2
Case I Test 3	1038	1	No. 2
Case II Test 1	1119	1	No. 3
Case II Test 2	1072	2	No. 2
Case II Test 3	421	1	No. 3
Case III Test 1	1142	3	No. 3
Case III Test 2	944	1	No. 3
Case III Test 3	578	1	No. 1

The pressure behavior with time is similar for every test, with the maximum pressures recorded (at fracture initiation) within a very close range (1038-1142 psi) for all except three tests. The maximum pressure reached in Case III Test 2 was a little below that range at 944 psi. Case II Test 3 and Case III Tests 3 had maximum pressure recorded significantly lower from that range; 421 and 578 psi, respectively.

4.3   Discussion

4.3.1   Fracture Growth Homogeneity Analysis

The homogeneity of fracture growth for each test is quantified by using the method outlined in Chapter 3, Section 3.5. The fracture length is the sole parameter used for this characterization and the fracture length homogeneity factor (*FLHF*) is calculated for each test, is shown on Tables 4.2a-c. It should be noted that the *FLHF* for tests with three perforations present, in which only one fracture was generated is always 1/3.

Table 4.2a – Fracture growth homogeneity analysis for Case I.

Parameters	Test 1	Test 2	Test 3
l_1 (in)	0.79	0.59	0
l_2 (in)	0.98	0.59	1.57
l_3 (in)	1.57	1.38	0
N_1^{length}	0.5	0.43	0
N_2^{length}	0.63	0.43	1
N_3^{length}	1	1	0
D_1^1 (in)	0	0	0
D_1^2 (in)	3.5	3.5	3.5
D_1^3 (in)	7	7	7
$N_1^{position}$	0	0	0
$N_2^{position}$	0.5	0.5	0.5
$N_3^{position}$	1	1	1
FLHF	0.71	0.62	0.33

Table 4.2b – Fracture growth homogeneity analysis for Case II.

Parameters	Test 1	Test 2	Test 3
l_1 (in)	0	0	0
l_2 (in)	0	0.59	0
l_3 (in)	1.57	1.38	1.38
N_1^{length}	0	0	0
N_2^{length}	0	0.43	0
N_3^{length}	1	1	1
D_1^1 (in)	0	0	0
D_1^2 (in)	2	2	2
D_1^3 (in)	7	7	7
$N_1^{position}$	0	0	0
$N_2^{position}$	0.29	0.29	0.29
$N_3^{position}$	1	1	1
FLHF	0.33	0.48	0.33

Table 4.2c – Fracture growth homogeneity analysis for Case III.

Parameters	Test 1	Test 2	Test 3
$l_1\ (in)$	1.18	0	0.79
$l_2\ (in)$	0.98	0	0
$l_3\ (in)$	0.39	1.57	0
N_1^{length}	1	0	1
N_2^{length}	0.83	0	0
N_3^{length}	0.33	1	0
$D_1^1\ (in)$	0	0	0
$D_1^2\ (in)$	5	5	5
$D_1^3\ (in)$	7	7	7
$N_1^{position}$	0	0	0
$N_2^{position}$	0.71	0.71	0.71
$N_3^{position}$	1	1	1
FLHF	0.72	0.33	0.33

As mentioned before the *FLHF* is a strong varies with time during non-uniform fracture propagation. In order to make accurate comparisons ensuring that reliable conclusions are drawn, the *FLHF* for each is calculated at the point, just before the longest fracture reaches the specimen boundary on its surface, where the contact with the overburden load takes place. Figure 4.24 shows the snapshots of all nine tests at that point. Figure 4.25 shows the multiple fracture growth profile with respect to normalized fracture length for every test. The plot of *FLHF* against the normalized position of Perforation No. 2 is shown in Figure 4.26.
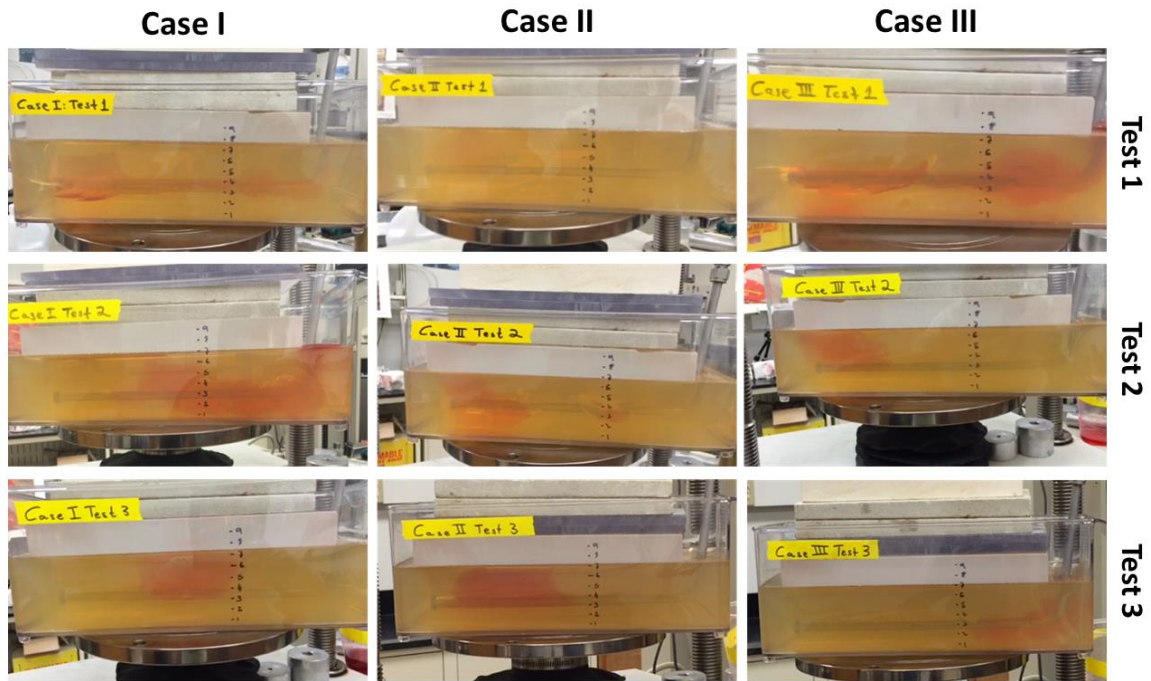
Figure 4.24 – Snapshots from all nine tests just before the first fracture reaches the specimen boundary at the surface. Case I, II and III are on column 1, 2 and 3 respectively and Test 1 and 2 and 3 are on row 1, 2 and 3 respectively.
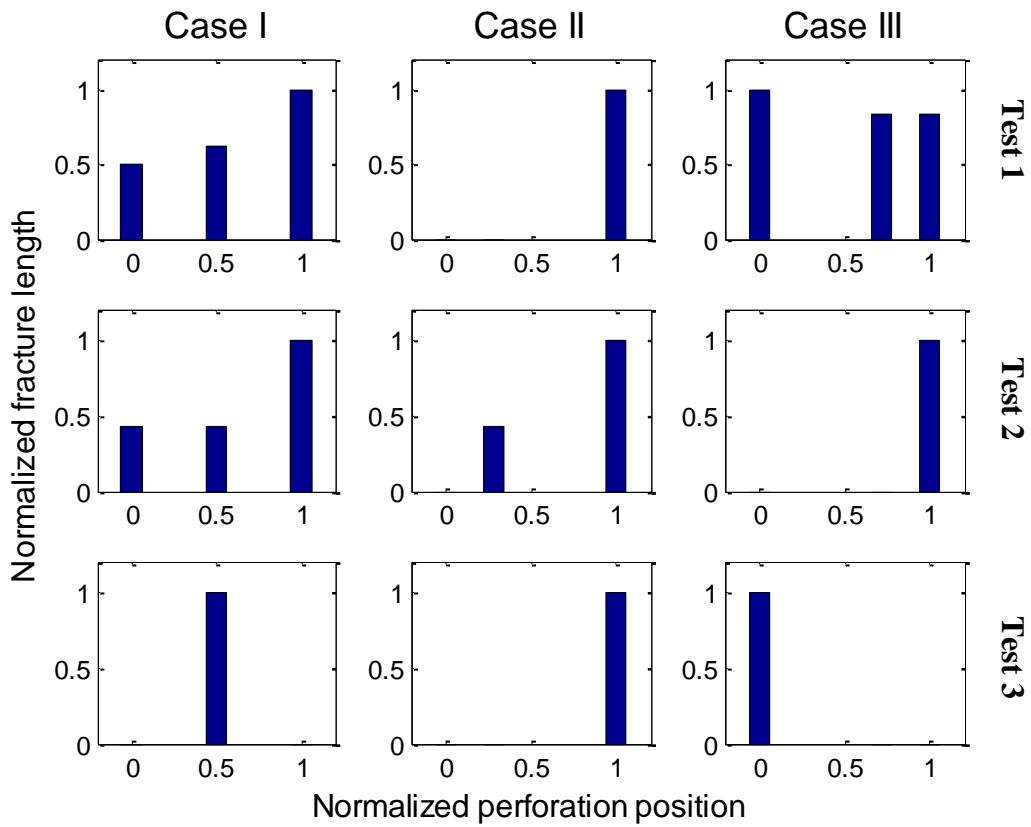
Figure 4.25 – Fracture growth profiles for the nine tests, showing the normalized length versus normalized position of the perforation from which each generated fracture was initiated.
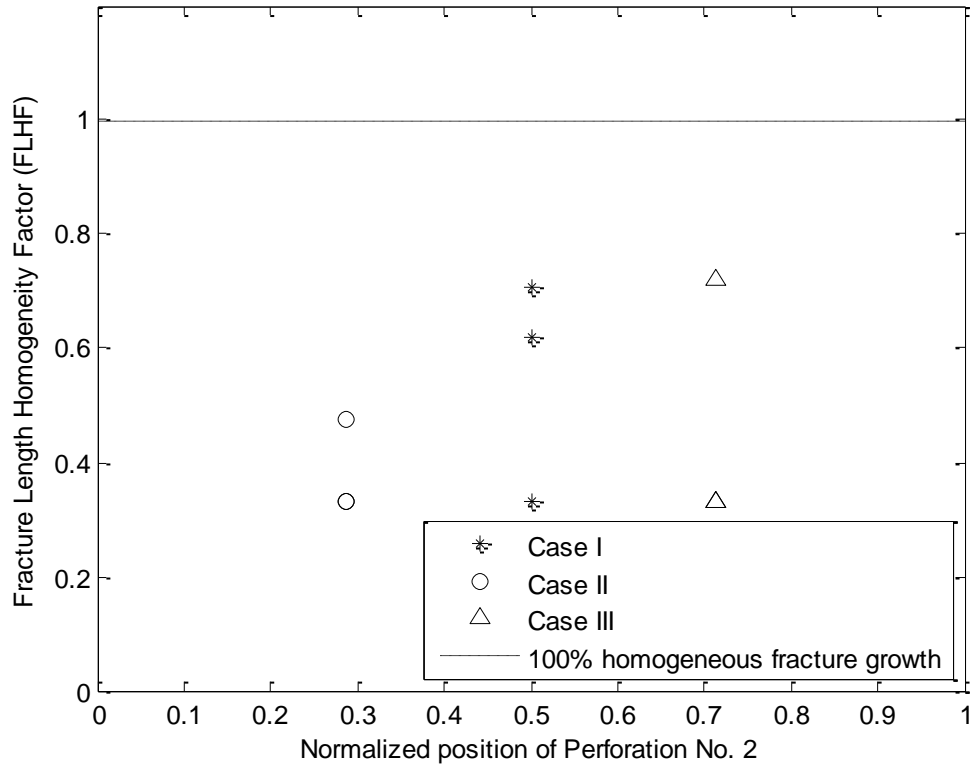
Figure 4.26 – Fracture length homogeneity factor versus normalized position for the nine tests.

The average (arithmetic mean) *FHLF* is then calculated for each of the three cases and they are tabulated on Table 4.3, along with the standard deviations. Figure 4.27 shows a plot of these average *FLHF* values against the normalized position of the middle perforation. A polynomial curve is then fitted between the points.

Table 4.3 – Average results per case.

Case	$N_2^{position}$	Average *FLHF*	Standard deviation
I	0.5000	0.5536	0.1959
II	0.2857	0.3810	0.0825
III	0.7143	0.4630	0.2245
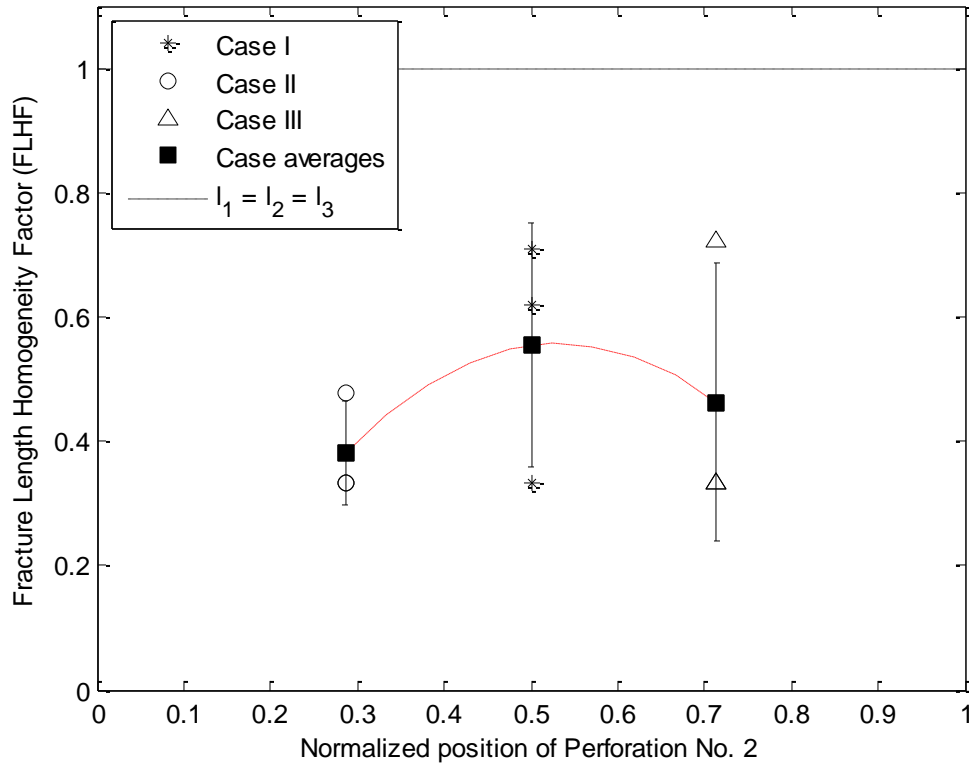
Figure 4.27 – Average fracture length homogeneity factor versus normalized position for the three cases.

There is some inconsistency in the test results for each case. Tests of all three Cases produced a single fracture at least once. There was no test in which all 3 fractures were initiated at the same time; substantial delay was observed between fracture initiations in every test that produced more than one fracture. This can be explained, by considering the wellbore pressure at each perforation along the horizontal lateral. The wellbore pressure in Perforation No. 1 is higher to pressure in No. 2, which is higher than that in No. 3, because of the fluid injected in that direction (from Perforation No. 1 to No. 3). This along with irregularities in the bonding between the wellbore and the gelatin, determine how many fractures will be generated and if more than one, at which sequence.

Assuming a constant value of gelatin breakdown pressure in all three perforations it means that the wellbore pressure at the first perforation (No. 1) will reach the gelatin

breakdown pressure before No. 2 and No. 3. Figure 4.28 shows conceptually how the relationship between wellbore and breakdown pressures changes with injection time at three different time steps; $t+\Delta t_1$, $t+\Delta t_2$ and $t+\Delta t_3$, where t is the time at which injection begins and $\Delta t_1 < \Delta t_2 < \Delta t_3$.
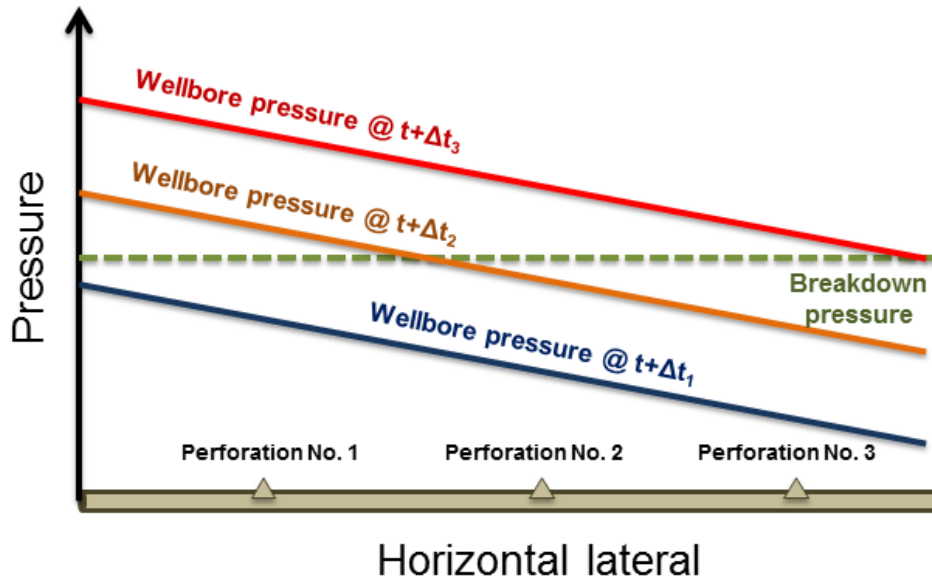
Figure 4.28 – Schematic of wellbore and breakdown pressure profiles along a horizontal lateral during various time intervals of fluid injection ($t+\Delta t_1 < t+\Delta t_2 < t+\Delta t_3$).

As the fluid is injected, the wellbore pressure increases and, theoretically, the slope stays constant. According to the Hagen-Poiseulle equation for flow of a Newtonian through a cylindrical tube and neglecting gravity (Bird et al., 2002), it will be equal to,

$$\frac{\Delta P}{L} = \frac{8Q\mu}{\pi R^4} \tag{4.1}$$

where $\frac{\Delta P}{L}$ is the average pressure gradient, Q is the flow rate, R is the radius of the cylindrical tube and μ is the viscosity oif the fluid.

At time $t+\Delta t_1$ the wellbore pressure at all three perforations is lower than the breakdown pressure. Later at time $t+\Delta t_2$, the wellbore pressure at Perforation No. 1

surpasses the breakdown pressure and a fracture is been initiated there. However, at Perforations No. 2 and No. 3, the wellbore pressure is still lower than breakdown, thus no fractures are being initiated there. Finally, at time $t+\Delta t_3$ wellbore pressure in all three perforations is higher than breakdown pressure and all three fractures have been generated.

This phenomenon was observed in all three Pilot Tests using dyed Vaseline for fracturing fluid, where the first perforation near the heel of the lateral generated the dominant fractures, taking almost all the injected fluid (Figures 3.6a-c). The much higher viscosity of Vaseline compared to glycerin, make the pressure gradients generated in the wellbore (Equation 4.1) much higher, as well as the differences in pressure between the three perforations more significant (higher wellbore pressure slope compared to that for glycerin). Figure 4.29 shows a schematic of the wellbore pressure along the horizontal lateral for water, glycerin and Vaseline fluids for the same bottomhole pressure at the heel. Furthermore, the compressibility of the two fluids may affect their corresponding wellbore pressure profiles yielding variable slopes.
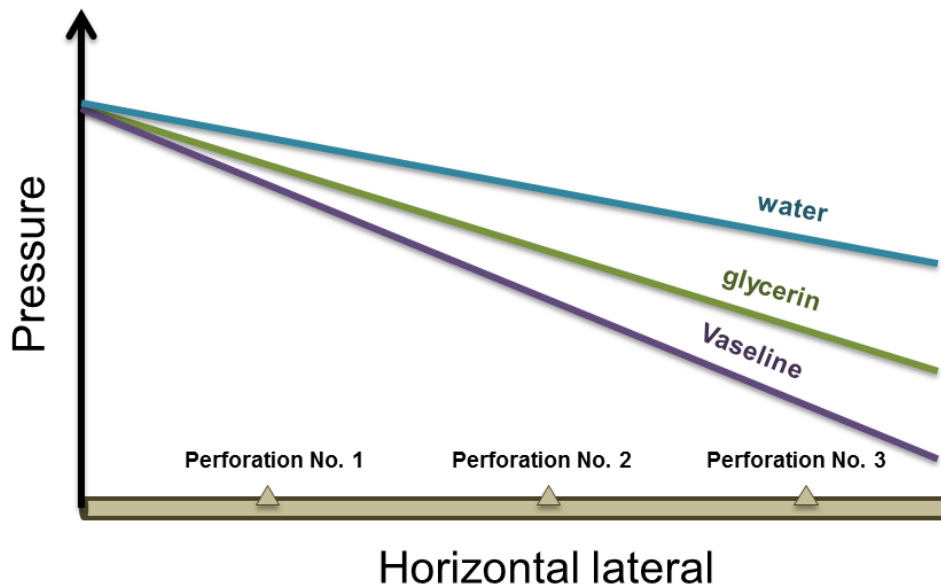
Figure 4.29 – Schematic of the wellbore pressure profile along a horizontal lateral for the three fracturing fluids: water, glycerin and Vaseline.

About half of the tests (five out of nine) generated only one fracture. The timing between the fracture initiations is most likely the biggest factor. Fracture fluid behaving analogously to electric current, choosing the path of least resistance to flow (Wu et al., 2015) would prefer to keep flowing through an existing fracture, propagating it, rather than initiating a new fracture from another perforation. This is because the fracture initiation pressure, assuming to be equal to the breakdown pressure of gelatin in this case, is higher than the fracture propagation pressure. Figure 2.5 shows qualitatively the pressure variation with respect to time expected during a hydraulic fracturing job.

Case I appears to be the one which promotes the most homogeneous fracture distributions. Case II is the worst of the three; producing very non-homogeneous fracture growth. Case III gave one test with 3 fractures, but the other two only one fracture was generated. Additional tests with this configuration would help clarify to what extent this is repeatable. These results imply that maximum spacing between perforations (Case I) minimize stress shadow effects more efficiently than non-uniform perforation arrays placing the middle perforation in locations of higher, (Case II) or lower wellbore pressure. Maximum spacing between the perforations also seems to promote production of more than one fracture from a single perforation, as happened in Case I tests.

The polynomial curve fitted in the plot (Figure 4.27) of the average *FLHF* of each of the three Cases, suggests that maximum *FLHF* of 0.56 will be achieved at the optimum normalized Perforation No. 2 position of 0.53.

4.3.2 Agreement with Theoretical Models

Absolute comparisons with numerical simulation modeling from the literature cannot be made, as most of those models are for four, (Wu et al., 2015) five and six (Peirce and Bunger, 2015) perforation cluster arrays. Nevertheless, comparing qualitatively the results of our tests to the trends shown in their simulations major discrepancies are observed.

Most importantly, varying the distance between perforations does not seem to balance out the stress shadow in comparison to when the distance is maximized (uniform

perforation array). The time delay between the initiations of different fractures, which is not considered in those simulations, is believed to be a major factor. Moreover, the decreasing wellbore pressure along the horizontal lateral justifies the non-symmetric length profile of fractures generated in the lateral compared to the models that predict a symmetric profile, due to the assumption of constant pressure in the horizontal wellbore.

4.3.3   Agreement with Field Data

In every test, regardless of the number of fractures generated, one fracture ends up dominating in terms of geometry propagation speed. Assuming proppant is placed in every fracture produced, making the permeability of these fractures higher than that of the surrounding rock formation, then this supports Miller et al.'s (2011) findings that the majority of production comes from very few perforation clusters.

Furthermore, all tests except one showed the dominant fracture was an exterior one, supporting field studies claiming that the middle clusters experience restricted fracture growth (Molenaar et al., 2012; Koskella et al., 2014). It also provides evidence supporting other studies that showed uneven distribution of fracturing fluid favoring the outer perforation clusters (Holley et al., 2010; Molenaar et al., 2012).

CHAPTER 5

CONCLUSIONS AND FUTURE WORK

5.1   Conclusions

The goal of the experimental program was to investigate the hypothesis that non-uniformly spaced, asymmetric perforation cluster arrays promotes more homogeneous fracture growth than uniformly spaced arrays. Based on the tests results obtained, the following conclusions are drawn.

- None of the non-uniform perforation array Cases (II and III) promoted better fracture growth homogeneity compared to the uniform base Case (I). Placing the middle perforation closer to the heel, or the toe of the horizontal lateral seems not to suppress stress shadow effects any better than when having maximum spacing across the three perforations. However, Case III was the only one that had at least in one test all three perforations initiating fractures. More test repetitions are needed to show what the probability of this occurrence may be.

- Fracturing fluid can bypass perforation(s) generating fractures in perforations further downstream on a horizontal well. This can happen both with an "inert" perforation between two "active" ones and an "inert" perforation upstream or downstream of "active" one(s).

- The time delay in fracture initiation from different perforations is significant and is usually neglected in numerical modeling. The presence of a fracture alters the stress regime around it creating a stress shadow effect which disturbs the initiation and propagation of another fracture. More sophisticated numerical models should incorporate wellbore pressure gradient along the horizontal lateral and the subsequent time delay in multiple fracture initiation it causes.

- In about half of the tests, just one fracture was produced. In the other cases more than one was produced, but in every test there was a "dominant" fracture whose growth and geometric dimensions are significantly greater compared to those of the other fractures. Assuming improved oil and gas flow due to increases in permeability, due to the addition of proppant in the fracture, this agrees with field work data (Miller et al., 2011) showing the majority of production coming from only a few perforation clusters.
- "Dominant" fractures were initiated mainly from the exterior Perforations No. 1 and No. 3. However, the interior Perforation No. 2 also produced a "dominant" fracture once with Case I.
- The fracturing fluid does not reach the crack tip. Air present in the wellbore prior to the placement of fracturing fluid gets compressed during pumping and guides glycerin into the fracture.
- The data acquisition showed consistent variation of pressure in all the tests. It is impossible to visualize accurately what goes on in the specimen, just by looking at pressure, flow rate and injected volume parameters variation with time during the test. The low compressibility of the dyed glycerin is suspected to cause deviation in the actual pressure behavior from the expected (see Figure 2.5).

5.2   Future Work

Based on the conclusions drawn from this experimental program, two similar research projects are proposed as candidates for future work on hydraulic fracturing optimization. These are the investigation of potential stress shadow mitigation either by using the same perforation arrays, but pumping in a pre-determined sequence by perforation, or by using variable perforation diameters and uniform perforation spacing.

5.2.1 Experimental Investigation of Non-uniform Perforation Cluster Arrays with Separate Pumping per Perforation

In the tests performed it became evident that the sequence at which the perforations initiate fractures (or not) exhibits severe uncertainty. This has implication in the fracture initiation and propagation from the other perforations. The fracture propagation pressure being generally quite lower than the fracture initiation (breakdown) pressure (see Figure 2.5) makes the fluid more likely to prefer to propagate an existing fracture, rather than initiating a new one. The current experimental setup, with some slight modifications can enable the initiation of fractures from each perforation in sequence.

A movable plastic tube inside the aluminum wellbore plugged on the end with one perforation allows flow only through the wellbore perforation aligned with the perforation on the plastic tube. With this setup different sequence strategies suggested by theoretical models for the stimulation of multiple perforation clusters from a horizontal well may be tested (for example, Roussel and Sharma, 2011).

5.2.2 Stress Shadow Mitigation via Perforation Diameter Variation

The next step proposed to optimize hydraulic fracturing is to observe whether the stress shadow effect can be balanced out, making multiple fracture growth more homogeneous, by varying the perforation diameter. The numerical simulation study of Wu et al. (2015) has suggested that control of the flow rate distribution into each perforation cluster can rectify uneven fracture growth. Decreasing the diameter of the outer perforations causes effective limited entry perforation friction, which balances the uneven fluid flow distribution, favoring the outer perforations. The same experimental setup can be used with wellbores of three evenly spaced perforations, as in Case I. Different diameters of each perforation could be tested.

Glossary

l_i = length of ith fracture

l_{max} = maximum fracture length achieved in the test

N_i^{length} = normalized length of ith fracture

$FLHF$ = Fracture Length Homogeneity Factor

D_i^j = distance from jth perforation to ith perforation

$N_i^{position}$ = normalized position of ith fracture

S_i = principal stress, where i = 1, 2 and 3 in accordance to relative magnitude

S_v = vertical principal in − situ stress

S_{Hmax} = maximum horizontal principal in − situ stress

S_{hmin} = minimum horizontal principal in − situ stress

p_p = pore pressure

σ_i = effective principal stress, where i = 1, 2 and 3 = $S_i - p_p$

T = tensile strength

q_{inj} = fracturing fluid injection

r_f = fracture radius

G = shear modulus

ν = Poisson's ratio

μ = fluid viscosity

w = fracture width

w_w = fracture width at wellbore

p_{frac} = fracture pressure

$p_{net}^{average}$ = average fracture net pressure = $p_{frac} - p_p$

E = Young's modulus

L = fracture half length

h = fracture height

References

Al Abbad, E. A., 2014, Experimental Investigation of Geomechanical Aspects of Hydraulic Fracturing Unconventional Formations, Master's Thesis at the University of Texas at Austin.

Anderson, T. L. *Fracture Mechanics: Fundamentals and Applications*. Boca Raton: CRC, 1995. Print.

Asiamah, N. K. S., 2015, Multi-frac Propagation in Unconventional Shale, Master's Thesis at the University of Texas at Austin.

Bahorich, B., Olson, J. E., & Holder, J. (2012, January 1). Examining the Effect of Cemented Natural Fractures on Hydraulic Fracture Propagation in Hydrostone Block Experiments. Society of Petroleum Engineers. doi:10.2118/160197-MS

Bird, R. Byron, Warren E. Stewart, and Edwin N. Lightfoot. *Transport Phenomena*. New York: J. Wiley, 2002. Print.

Crosby, D.G., M.M. Rahman, M.K. Rahman, and S.S. Rahman. "Single and Multiple Transverse Fracture Initiation from Horizontal Wells." *Journal of Petroleum Science and Engineering* 35.3-4 (2002): 191-204. Web. 28 Feb. 2016.

"Crystal Clear® Series Clear Urethane Casting Resins." Smooth-on, Inc., n.d. Web. 28 Feb. 2016. <http://www.smooth-on.com/tb/files/CRYSTAL_CLEAR_200_TB.pdf>.

De Pater, C. J., Cleary, M. P., Quinn, T. S., Barr, D. T., Johnson, D. E., & Weijers, L. (1994, November 1). Experimental Verification of Dimensional Analysis for Hydraulic Fracturing. Society of Petroleum Engineers. doi:10.2118/24994-PA

Economides, Michael J., A. D. Hill, and Christine Ehlig-Economides. *Petroleum Production Systems*. Englewood Cliffs, NJ: PTR Prentice Hall, 1994. Print.

El Rabaa, W. (1987, January 1). Hydraulic Fracture Propagation in the Presence of Stress Variation. Society of Petroleum Engineers. doi:10.2118/16898-MS

El Rabaa, W. (1989, January 1). Experimental Study of Hydraulic Fracture Geometry Initiated From Horizontal Wells. Society of Petroleum Engineers. doi:10.2118/19720-MS

Fisher, M. K., Heinze, J. R., Harris, C. D., Davidson, B. M., Wright, C. A., & Dunn, K. P. (2004, January 1). Optimizing Horizontal Completion Techniques in the Barnett Shale Using Microseismic Fracture Mapping. Society of Petroleum Engineers. doi:10.2118/90051-MS

Frash, L. P., 2014, Laboratory-scale Study of Hydraulic Fracturing in Heterogeneous Media for Enhanced Geothermal Systems and General Well Stimulation, PhD Thesis at Colorado School of Mines.

Frash L, Hood J, and Gutierrez M, 2013. Hydraulic fracture visualization: fracking acrylic with epoxy. http://youtu.be/lTPY-KuUv2E. (accessed 28 February 2016)

Frash, L. P., Hood, J., Gutierrez, M., Huang, H., & Mattson, E. (2014, August 18). Laboratory Measurement of Critical State Hydraulic Fracture Geometry. American Rock Mechanics Association.

Fu, Y., 2014, Leak-Off Test (LOT) Models, Master's Thesis at the University of Texas at Austin.

Geertsma, J. and de Klerk, F. A. 1969. A rapid method of predicting width and extent of hydraulically induced fractures. J. Petroleum Technology 21(12): 1571-1781.

Groenenboom, J., van Dam, D. B., & de Pater, C. J. (1999, January 1). Time lapse ultrasonic measurements of laboratory hydraulic fracture growth: width profile and tip behaviour. Society of Petroleum Engineers. doi:10.2118/56727-MS

Haimson, B., & Fairhurst, C. (1967, September 1). Initiation and Extension of Hydraulic Fractures in Rocks. Society of Petroleum Engineers. doi:10.2118/1710-PA

Hoek, E., Brown, E.T., 1980. Empirical strength criterion for rock masses. Journal of Geotechnical Engineering Division, ASCE 106 (GT9), 1013– 1035.

Holley, E. H., Zimmer, U., Mayerhofer, M. J., and Samson, E., 2010, Integrated Analysis Combining Microseismic Mapping and Fiber-Optic Distributed Temperature

Sensing (DTS), CSUG/SPE 136565, the Canadian Unconventional Resources and International Petroleum Conference, Calgary, Alberta, Canada, October 19-21.

Hubbert, M. K., & Willis, D. G. (1957, January 1). Mechanics Of Hydraulic Fracturing. Society of Petroleum Engineers.

Kirsch, G., 1898. Die theorie der elasticitaet und die beduerfnisse der festigkeitskehre. VDI-Z 42, 707.

Koskella, D., 2014, Observations from an Underground Laboratory: An Integrated Diagnostic Approach to Unlocking Performance in the Niobrara, Keynote Speech, the SPE Hydraulic Fracturing Technology Conference, The Woodlands, TX, USA, February 4-6.

Miller, C. K., Waters, G. A., & Rylander, E. I. (2011, January 1). Evaluation of Production Log Data from Horizontal Wells Drilled in Organic Shales. Society of Petroleum Engineers. doi:10.2118/144326-MS

Molenaar, M. M., Fidan, E., & Hill, D. (2012, January 1). Real-Time Downhole Monitoring Of Hydraulic Fracturing Treatments Using Fibre Optic Distributed Temperature And Acoustic Sensing. Society of Petroleum Engineers. doi:10.2118/152981-MS

Nagel, N., Gil, I., Sanchez-Nagel, M., and Damjanac, B., Simulating Hydraulic Fracturing in Real Fractured Rock – Overcoming the Limits of Pseudo 3D Models, SPE 140480, the SPE Hydraulic Fracturing Technology Conference, The Woodlands, TX, USA, January 24-26.

Nagel, N., Sheibani, F., Lee, B., Agharazi, A., and Zhang, F., 2014, Fully-Coupled Numerical Evaluations of Multiwell Completion Schemes: The Critical Role of InSitu Pressure Changes and Well Configuration, SPE 168581, the SPE Hydraulic Fracturing Technology Conference, The Woodlands, TX, USA, February 4-6.

Nordgren, R. P.1972. Propagation of a vertical hydraulic fracture. SPE 3009-PA. Society of Petroleum Engineering Journal 12(4): 306-314.

Olson, J. E., 2008, Multi-Fracture Propagation Modeling: Applications to Hydraulic Fracturing in Shales and Tight Gas Sands, ARMA 08-327, the 42nd US Rock

Mechanics Symposium and 2nd US-Canada Rock Mechanics Symposium, San Francisco, CA, USA, June 29-July 2.

Olson, J. E., and Wu, K., 2012, Sequential Versus Simultaneous Multi-Zone Fracturing in Horizontal Wells: Insights from a Non-Planar, Multi-Frac Numerical Model, SPE 152602, the SPE Hydraulic Fracturing Technology Conference, The Woodlands, TX, USA, February 6-8.

Peirce, A., & Bunger, A. (2015, April 1). Interference Fracturing: Nonuniform Distributions of Perforation Clusters That Promote Simultaneous Growth of Multiple Hydraulic Fractures. Society of Petroleum Engineers. doi:10.2118/172500-PA

Perkins, T. K. and Kern, L. R.1961. Width of hydraulic fractures. J. Petroleum Technology 13(9): 937-949.

Roussel, N. P., & Sharma, M. M. (2011, May 1). Optimizing Fracture Spacing and Sequencing in Horizontal-Well Fracturing. Society of Petroleum Engineers. doi:10.2118/127986-PA

Shin, D. H., and Sharma, M. M., 2014, Factors Controlling the Simultaneous Propagation of Multiple Competing Fractures in a Horizontal Well, SPE 168599, the SPE Hydraulic Fracturing Technology Conference, The Woodlands, TX, USA, February 4-6.

The Shale Revolution. Publication. Credit Suisse Securities Research & Analytics, 25 Feb. 2014. Web. 16 Nov. 2015.

United States. Department of Energy. Office of Fossil Energy National Energy Technology Laboratory. *Modern Shale Gas Development in the United States: A Primer*. N.p., 1 Apr. 2009. Web. 15 Nov. 2015.

"U.S. Energy Information Administration - EIA - Independent Statistics and Analysis." *U.S. Energy Information Administration (EIA)*. N.p., n.d. Web. 27 Jan. 2016.

Valkó, Peter, and Michael J. Economides. *Hydraulic Fracture Mechanics*. Chichester: Wiley, 1995. Print.

Wu, H., Golovin, E., Shulkin, Y., Chudnovsky, A., Dudley, J. W., & Wong, G. K. (2008, January 1). Observations of Hydraulic Fracture Initiation and Propagation in a Brittle Polymer. American Rock Mechanics Association.

Wu, K., Olson, J., Balhoff, M. T., & Yu, W. (2015, September 28). Numerical Analysis for Promoting Uniform Development of Simultaneous Multiple Fracture Propagation in Horizontal Wells. Society of Petroleum Engineers. doi:10.2118/174869-MS

Xu, G., & Wong, S.-W. (2013, March 26). Interaction of Multiple Non-Planar Hydraulic Fractures in Horizontal Wells. International Petroleum Technology Conference. doi:10.2523/17043-MS

Zoback, Mark D. *Reservoir Geomechanics*. Cambridge: Cambridge UP, 2007. Print.

Vita

Andreas Michael was born in Larnaca, Cyprus in 1989. After completing his secondary school studies in the American Academy of Larnaca he joined the Cyprus National Guard for two years of mandatory military service. In August 2010, he enrolled in the petroleum engineering program at The University of Texas at Austin, receiving his Bachelor's degree in December 2013, continuing as a graduate student since. He has a broad knowledge on the discipline and the industry having represented the school internationally at the SPE PetroBowl Championship for three years in a row reaching 2nd place in 2013 and 2015. His professional interests include petroleum geomechanics, petrophysics, economics and geopolitics.

Permanent address: 7 Delacrouax Street, Larnaca, Cyprus 6052

Email address: andreasmichael89@yahoo.com

This report was typed by the author.